MICROPOROUS COORDINATION POLYMERS AS SELECTIVE ADSORBENTS FOR COMPLEX MATRICES

by

Katie A. Cychosz

A dissertation submitted in partial fulfillment
of the requirements for the degree of
Doctor of Philosophy
(Chemistry)
in The University of Michigan
2010

Doctoral Committee:

Professor Adam J. Matzger, Chair
Professor John Montgomery
Professor Levi T. Thompson, Jr.
Associate Professor Melanie S. Sanford

ACKNOWLEDGEMENTS

I would like to thank my advisor, Professor Adam Matzger, for his guidance and support during my graduate studies. I am also thankful to my committee members, Professor Melanie Sanford, Professor John Montgomery, and Professor Levi Thompson, for their time and commitment to me during my graduate career. This research project was only accomplished with help and input from many others who also deserve recognition. I would particularly like to thank Dr. Antek Wong-Foy for getting me started on this project and for being there to help throughout the years. Thank you to Dr. Tae-Hong Park for synthesizing the UMCM-150$(N)_1$ and UMCM-150$(N)_2$ and to Ms. Jenny Schnobrich for synthesizing the UMCM-152 and UMCM-153 that I worked with. I am also appreciative of the help and friendship from current and past members of the Matzger group.

I am eternally grateful for the support and encouragement from my family, especially my parents Roy and Kay Cychosz. Additionally, I would like to thank my good friends Ms. Claire Farnsworth and Ms. Therese Dorau for always being just a phone call away when I needed them.

TABLE OF CONTENTS

LIST OF FIGURES

Figure

LIST OF SCHEMES

Scheme

ABSTRACT

Crystalline microporous coordination polymers (MCPs) are ordered, porous materials that have recently seen increasing attention in the literature. Whereas gas phase separations using MCPs have been extensively studied and reviewed, studies on applications in the liquid phase, particularly from complex matrices, have lagged behind. In this thesis, MCPs have been applied to adsorption from diesel and water.

The utility of MCPs for the adsorption of large organosulfur compounds (benzothiophene, dibenzothiophene, 4,6-dimethyldibenzothiophene) found as pollutant precursors in fuels was demonstrated. Large capacities were obtained, particularly for 4,6-dimethyldibenzothiophene, the compound most difficult to remove using current industrial techniques. It was determined that the size/shape of the pores in the MCP, rather than surface area or pore volume, is the most important factor controlling adsorption capacity. This was confirmed by studying the supramolecular isomers University of Michigan Crystalline Material (UMCM)-152 and UMCM-153 which exhibited different adsorption behaviors. Electron-deficient MCPs were also tested and higher adsorption capacities were observed for the most electron-deficient structure.

MCPs were demonstrated to be efficient adsorbents for the removal of the organosulfur compounds dibenzothiophene (DBT) and 4,6-dimethyldibenzothiophene (DMDBT) from model fuel and diesel fuel in packed bed breakthrough experiments. Unlike activated carbons, where selectivity has been a problem, MCPs selectively adsorb

the organosulfur compounds over similar components of diesel. Complete regeneration using toluene at modest temperatures was achieved. The attainment of high selectivities and capacities, particularly for the adsorption of the difficult to remove refractory compounds, in a reversible sorbent indicates that fuel desulfurization may be an important application for MCPs.

Finally, the water stability of a variety of MCPs was studied using powder X-ray diffraction. It was determined that the stability of the MCP is related to the metal cluster present in the structure with trinuclear chromium clusters more stable than copper paddlewheel clusters which are more stable than basic zinc acetate clusters. Matériaux de l'Institut Lavoisier (MIL)-100 was found to be completely water stable and was used to adsorb the pharmaceuticals furosemide and sulfasalazine from water with large uptakes at low concentrations, indicating that the adsorption of wastewater contaminants may be a feasible application for these materials.

CHAPTER 1

Introduction

1.1. Adsorption in Porous Materials

Adsorption represents a large and growing area of separations technologies impacting sectors ranging from pharmaceuticals and fine chemicals to the petrochemical industry. The market for sorbents is currently valued around $3 billion annually[1] and virtually all of the sorbents used in these applications are from one of three general classes of materials: activated carbons (including carbon molecular sieves), zeolites (natural and synthetic), and metal/metalloid oxides including silica gel and activated alumina. Zeolites are crystalline materials with highly ordered pore structures whereas activated carbons, aluminas, and silicas are amorphous with variable pore size distributions. However, the key characteristic common to these materials is that all exhibit microporosity. A fourth category of adsorbents has the promise to revolutionize adsorption technologies; crystalline microporous coordination polymers (MCPs) are an exciting new class of highly ordered porous materials that combine the well-defined structural characteristics of zeolites with surface areas exceeding those of the best activated carbons.

1.2 Microporous Coordination Polymers

MCPs are referred to in the literature by a number of different names including metal-organic framework (MOF), porous coordination polymer (PCP), and porous coordination network (PCN), as well as by names which refer to the location where the material was originally synthesized such as Hong Kong University of Science and Technology (HKUST), Matériaux de l'Institut Lavoisier (MIL), Porphyrinic Illinois Zeolite Analogue (PIZA), and University of Michigan Crystalline Material (UMCM). These materials consist of metal ions or metal clusters assembled in a periodic fashion through organic ligands (referred to as linkers) resulting in an extended porous host structure. This style of assembly takes advantage of the directionality of the bonding between the metal atom and the linker and, in contrast to many zeolite preparations, avoids the need for a templating agent during synthesis. Like zeolites, very narrow pore size distributions can be obtained; however, this extremely high degree of control over pore size can be achieved over a much broader size range (3.5-34 Å are easily obtainable for MCPs). Compared to zeolites, metal oxides, or activated carbons, the dead volume or inaccessible space in MCPs is considerably diminished leading to the tremendous porosities and high surface areas observed. Brunauer-Emmett-Teller (BET) surface areas in excess of 5000 m^2/g and pore volumes reaching 2.3 cm^3/g have been obtained for MCPs.[2] Furthermore, incorporation of functional groups (e.g. halogen, nitrogen, sulfur, carboxy, cyano, nitro) on the organic linker, as well as the ability to select different metals, allows the electronic nature of the pore surface to be tuned, a feat very difficult to achieve in zeolites or activated carbons. Representative examples of the synthesis,

structure, and prior use of MCPs studied for liquid phase adsorption in this thesis are presented below.

1.2.1. MOF-5

MOF-5 is one of the first reported examples of an MCP in the literature and is comprised of basic zinc acetate metal clusters connected by 1,4-benzenedicarboxylate to form a three dimensional cubic structure (Scheme 1.1, Figure 1.1).[3] MOF-5 has a BET surface area of 3800 m^2/g[4] and is used as the prototypical standard zinc MCP to which subsequent MCPs and their adsorption properties are often compared.

1.2.2. HKUST-1

Like MOF-5, HKUST-1 is also one of the first examples of an MCP in the literature and consists of copper paddlewheel metal clusters linked by 1,3,5-benzenetricarboxylate (Scheme 1.2, Figure 1.2).[5] Recently commercialized by BASF, HKUST-1 has a BET surface area of 1900 m^2/g[6] and has been extensively studied in applications ranging from gas and liquid phase adsorption to catalysis as a prototypical copper MCP.

1.2.3. MOF-177

MOF-177, comprised of octahedral basic zinc carboxylate clusters linked by 1,3,5-(triscarboxyphenyl)benzene, was the first MCP reported to exceed the surface areas of the best activated carbons; moreover, the extremely high BET surface area (4700 m^2/g) of MOF-177 is accompanied by large pores leading to a pore volume of 1.59 cm^3/g (Scheme 1.3, Figure 1.3).[6,7] The pore aperture is sufficient to allow free diffusion of C_{60} through macroscopic MOF-177 crystals as evidenced by Raman spectroscopy.[7]

Additionally, MOF-177 is one of the best MCPs for hydrogen storage with a hydrogen uptake of 7.5 wt%.[6]

1.2.4. MOF-505

The reaction of copper nitrate with 3,3',5,5'-biphenyltetracarboxylic acid leads to the formation of the MCP MOF-505 (Scheme 1.4).[8] The structure consists of copper paddlewheel metal clusters and two different size and shaped pores and has a BET surface area of 1670 m^2/g (Figure 1.4).[9] MOF-505 has primarily been studied for hydrogen adsorption and its structure has inspired a series of MCPs with extended and/or functionalized 3,3',5,5'-biphenyltetracarboxylic acid organic linkers.[10]

1.2.5. UMCM-150

UMCM-150, comprised of copper paddlewheel and trinuclear copper metal clusters linked by 3,4',5-biphenyltricarboxylate, is one of the first examples of an MCP formed from an unsymmetrically substituted organic linker (Scheme 1.5, Figure 1.5).[11] Possessing a BET surface area of 2300 m^2/g, UMCM-150 consists of two different copper metal clusters and three types of cages. UMCM-150 is among the best materials for high pressure hydrogen uptake with volumetric hydrogen uptakes estimated at 36 g/L.[11] While studies on this new material have thus far been limited, it is one of the best MCPs for the desulfurization of transportation fuels as will be discussed in Chapters 2 and 3 of this thesis.

1.2.6. MIL-100

MIL-100 is formed from the reaction of chromium(IV) oxide and 1,3,5-benzenetricarboxylic acid (Scheme 1.6, Figure 1.6) and has a surface area of 3100 m^2/g.[12] MIL-100 consists of three distinct pores of different dimensions, two of which are

mesoporous. The uptake of gases such as methane,[13,14] hydrogen sulfide,[15] carbon dioxide,[14] and hydrogen[16] in MIL-100 has been explored. Additionally, ibuprofen has been loaded into MIL-100 and its properties for drug delivery have been studied.[17]

1.3. Liquid Phase Separations by Microporous Coordination Polymers

The potential for using MCPs as sorbents for separations is considerable and indeed, as shown in Figure 1.7, a range of molecules have been examined in the liquid phase. It is therefore surprising that as these novel sorbents head to market,[18,19] the bulk of the investigations involve gas adsorption. This contrasts strongly with more established sorbents where applications to liquid phase separations are in fact more prominent. Below are select, representative examples of liquid phase separations using MCPs.

1.3.1. Complex Mixtures

Porphyrinic Illinois Zeolite Analogue-1 (PIZA-1), which is comprised of ruffled cobalt(III) porphyrin cores connected by bridging trinuclear Co(II)-carboxylate clusters, demonstrated promise as a desiccant in the drying of the organic solvents benzene, toluene, and tetrahydrofuran.[20] In comparison with zeolite 4A, PIZA-1 exhibited very good capacity and affinity for water and displayed rapid kinetics for the selective sorption of water from organic solvent. In fact, PIZA-1 acted as a better desiccant in one hour than zeolite 4A did in 24 hours. Size and shape selectivity was also explored using a series of aromatic amines (to probe size selectivity) and both picolines and alcohols (to probe shape selectivity). In all cases, the smaller or less sterically bulky molecule was preferentially adsorbed. These studies revealed extraordinarily fast kinetics for guest

inclusion and, indeed, the fast kinetics of guest diffusion into MCPs seems to be a general phenomenon that offers MCPs significant advantages over zeolites.[19,21]

The competitive adsorption of the C_8 alkyl aromatic compounds ethylbenzene and all three isomers of xylenes from hexane was explored for the MCPs HKUST-1, MIL-47 (infinite chains of octahedral formed by coordination of V^{4+} by terephthalate and O^{2-} to produce a structure with one dimensional pores[22]), and MIL-53(Al) (infinite chains of octahedral formed by coordination of Al^{3+} by terephthalate and OH^- groups to produce a structure with one dimensional pores[23]) to probe the potential for isomer-selective adsorption.[24] HKUST-1 was selective only for *m*-xylene over *o*-xylene. The other two sorbents were much better at separating the C_8 alkyl aromatic compounds and had outstanding preferences for *p*-xylene over ethylbenzene. In pulse chromatographic experiments with MIL-47, separate peaks were obtained for ethylbenzene, *m*-xylene and *p*-xylene. The selectivities in MIL-47 were attributed to a molecular packing effect inside the sterically confining environment of the pores. This was the first example of an extremely industrially relevant separation application, as zeolites are often used for the separation of xylene isomers and these results illustrate that MIL-47 is also effective at separation of these isomers.

In a similar study, the adsorption of C_8 alkyl aromatic compounds from hexane on MIL-53, using batch and column adsorption techniques was explored and the results were compared with MIL-47.[25] MIL-53 had a particular preference for the adsorption of *o*-xylene, but was not able to discriminate between *m*- and *p*-xylene and did not adsorb ethylbenzene. In the pulse chromatographic experiments ethylbenzene eluted first, *m*- and *p*-xylene came simultaneously and *o*-xylene appeared last. In breakthrough experiments,

ethylbenzene breaks through after a very short time, then *m*-xylene, and, last, *o*-xylene. MIL-53 was also used for the adsorption of ethyltoluene and cymene isomers and again adsorption of the *ortho* isomer was preferred. It was found using powder X-ray diffraction that the geometry of *o*-xylene allows for interaction between both methyl groups with the carboxylate groups in the structure, interactions which are not as prevalent for the other isomers, suggesting that this is the reason for the observed selectivities. In a comparison between MIL-47 and MIL-53 for adsorption of C_8 alkyl aromatics, as mentioned earlier, MIL-47 preferred adsorption of *p*- and *m*-xylene over ethylbenzene and *o*-xylene and efficiently separated *p*- and *m*-xylene, in contrast to this study which showed that MIL-53 selectively adsorbs the *ortho* isomer and is unable to discriminate between the *para* and *meta* isomers. The two sorbents have almost identical pore topography indicating that the selectivities were instead due to the metals in the two sorbents leading to different polarization of the carboxylate groups. The dissimilar selectivities for differing metal ions substituted in the same framework topology make it convenient to separate the isomer of interest from a mixture. This example illustrates how changing one of the building blocks of an MCP can drastically change adsorption capacities in the context of an industrially relevant separation example.

HKUST-1 and MOF-5 were utilized as stationary phases for liquid chromatographic separations.[26] The size and shape selectivities of HKUST-1 were tested and it was found that in a mixture of benzene, naphthalene, and anthracene, the larger the aromatic compound, the longer the retention time due to greater interactions with the framework. Additionally, a mixture of benzene, naphthalene, and 1,3,5-triphenylbenzene was passed through the column and 1,3,5-triphenylbenzene was unretained due to size

exclusion. Again using HKUST-1, separation of ethyl benzene and styrene was very efficiently achieved. Unlike the previous case, here, separation is attributed to interactions between styrene and the copper of the framework by π-complexation, a conclusion further supported by attempting to use MOF-5 for the same separation. In this case, styrene and ethyl benzene co-elute due to the absence of coordinatively unsaturated metal sites in MOF-5. Furthermore, separations based on chemical interactions with the MCP may be useful for the separation of similarly sized molecules.

Not only can neutral molecules be separated using MCPs, but anions have also been separated from water using a luminescent porous framework.[27] I^-, Br^-, Cl^-, F^-, CN^-, and CO_3^{2-} were separated from aqueous solutions; however, SO_4^{2-} and PO_4^{2-} were not adsorbed because they were too large to fit inside the pores of the MCP. Adsorption was attributed to strong hydrogen bonding interactions between the anions and the OH groups on the mucic acid organic linkers. MCPs have also been used for the separation of the anions F^-, Cl^-, Br^-, CO_3^{2-}, or SO_4^{2-} from methanol.[28] Because of the potential for chemical interactions between guest anions and MCPs, separation of anions from solution is yet another attractive application for MCPs.

1.3.2. Enantiomers

There are only a handful of examples in the literature of the separation of enantiomers using MCPs. Notably, the highest enantiomeric excesses using MCPs to date were achieved with a zinc-metallosalen based material.[29] A racemic mixture of 2-butanol was efficiently separated due to selective inclusion of the *R*-isomer in the pores. Analysis revealed that an *ee* value of 99.8% was obtained. The *R* enantiomer of racemic 3-methyl-2-butanol was also selectively included with an *ee* of 99.6%. This work shows that it is

possible to design an MCP to almost perfectly resolve small racemic alcohols. Other enantiomer separations have been achieved with varying success including the resolution of $[Ru(2,2'\text{-bipyridyl})_3]Cl_2$,[30] binaphthol,[31] and a variety of racemic diols.[32] In most cases, higher *ee*'s were obtained with molecules that more closely matched the size and shape of the MCP pore.

Chromatographic separations have been used to resolve enantiomers of *trans*-1,2-diaminocyclohexane[33] and alkyl aryl sulfoxides.[34] In the case of the *trans*-1,2-diaminocyclohexane, only small enantioenrichments of 13.6% *S,S* in the beginning fractions were observed, indicating that new chiral MCPs need to be designed to make packed-bed separation of enantiomers feasible.

Even though there are examples of liquid phase separations using MCPs in the literature, extensive studies on complicated systems are lacking and are needed to fully understand the potential role that MCPs could play in this field. Further studies must be performed where (1) complex matrices are examined to determine the selectivity of MCPs for one component of a given mixture and (2) the separation of molecules from aqueous solutions are fully examined.

1.4. Organization of Thesis

Chapter 1 provides a general introduction to microporous coordination polymers. The current body of literature on liquid phase adsorption using MCPs is discussed.[35]

In Chapter 2, the benzothiophene, dibenzothiophene, and 4,6-dimethyldibenzothiophene equilibrium adsorption isotherms were measured for a variety

of MCPs. The effects of pore shape and size as well as linker electronics on the adsorption capacity were examined.[36,37]

In Chapter 3, the packed-bed breakthrough curves were determined for a variety of MCPs for the removal of dibenzothiophene and 4,6-dimethyldibenzothiophene from isooctane, isooctane/toluene, and diesel. Regeneration of the MCP packed beds was performed.[38]

In Chapter 4, the water stability of a variety of MCPs was investigated using powder X-ray diffraction. The adsorption of the pharmaceuticals furosemide and sulfasalazine from water using MCPs was then examined.

Chapter 5 is the conclusion of the thesis and provides some prospects for future research directions.

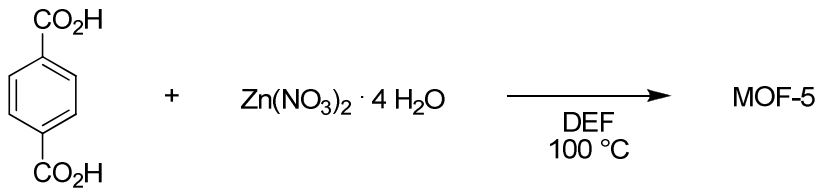

Scheme 1.1. Synthesis of MOF-5.

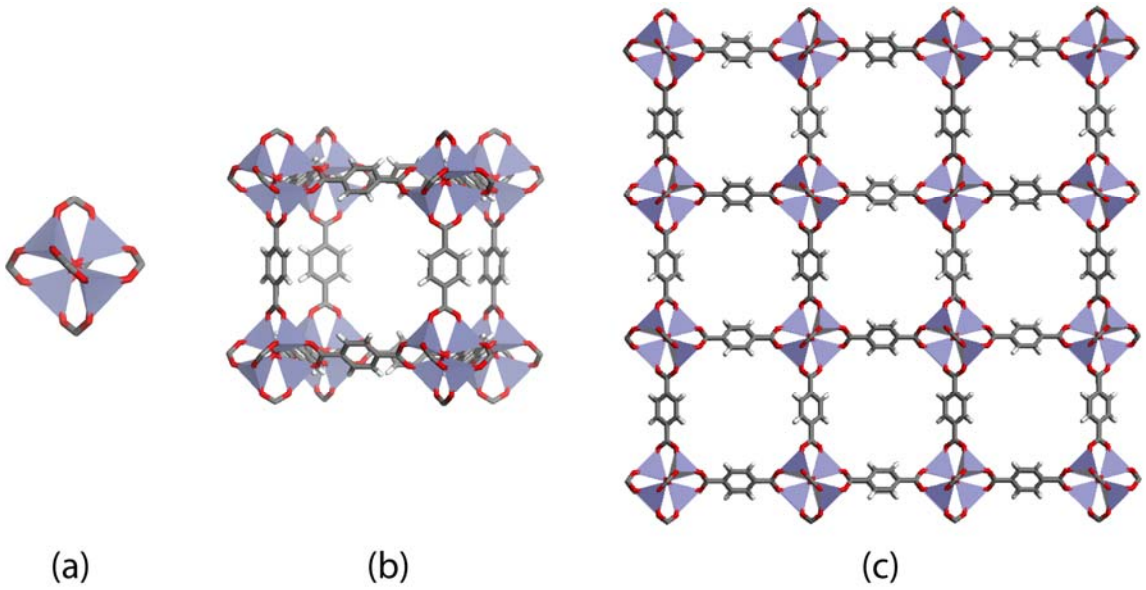

Figure 1.1. Crystal structure of MOF-5. (a) Zn_4O metal cluster, (b) one cage of MOF-5, and (c) the extended structure of MOF-5. C atoms (dark gray), H atoms (white), O atoms (red), Zn atoms (purple).

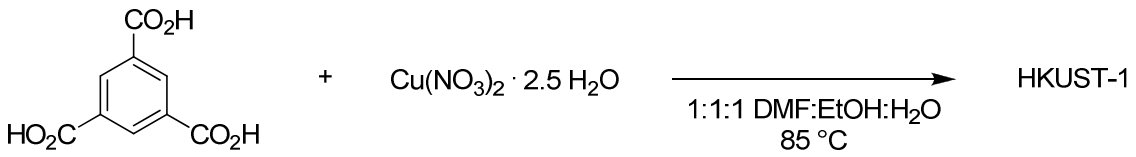

Scheme 1.2. Synthesis of HKUST-1.

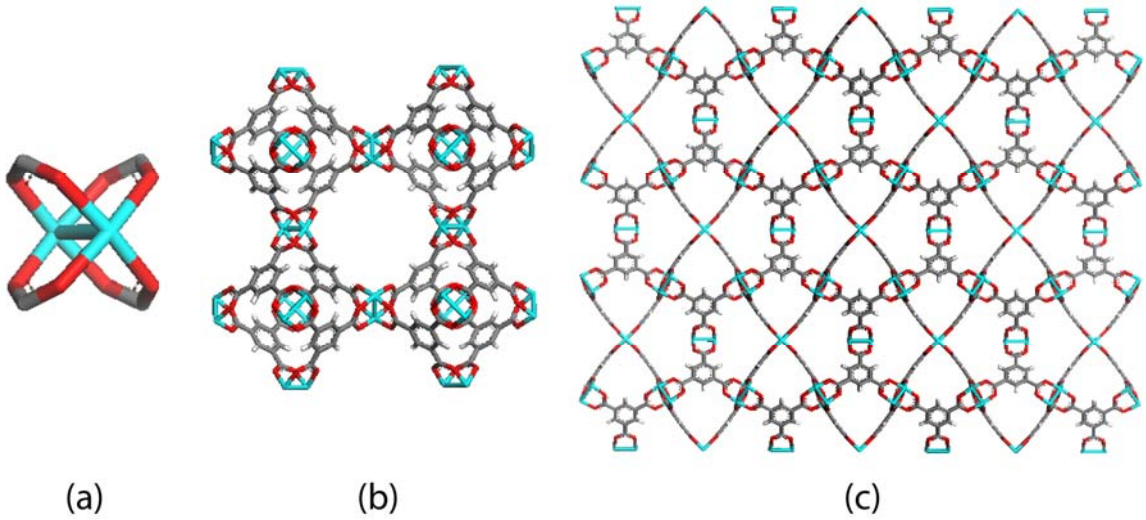

Figure 1.2. Crystal structure of HKUST-1. (a) Copper paddlewheel metal cluster, (b) view of HKUST-1 channels, and (c) the extended structure of HKUST-1. C atoms (dark gray), H atoms (white), O atoms (red), Cu atoms (blue).

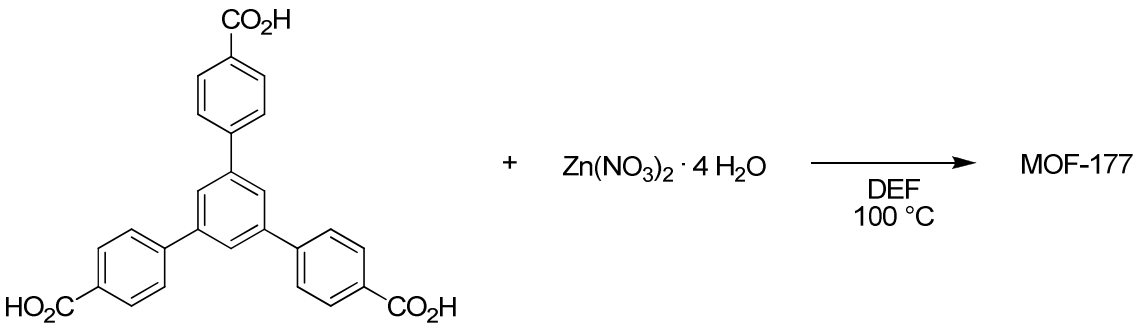

Scheme 1.3. Synthesis of MOF-177.

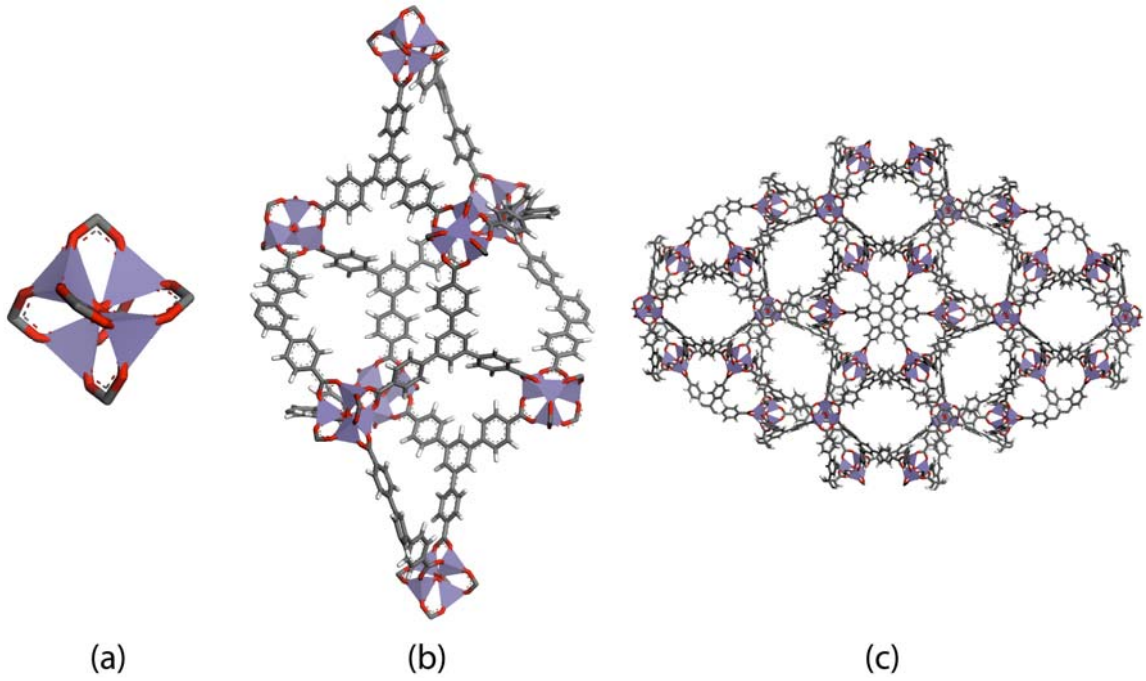

Figure 1.3. Crystal structure of MOF-177. (a) Zn_4O metal cluster, (b) view of MOF-177 cage, and (c) the extended structure of MOF-177. C atoms (dark gray), H atoms (white), O atoms (red), Zn atoms (purple).

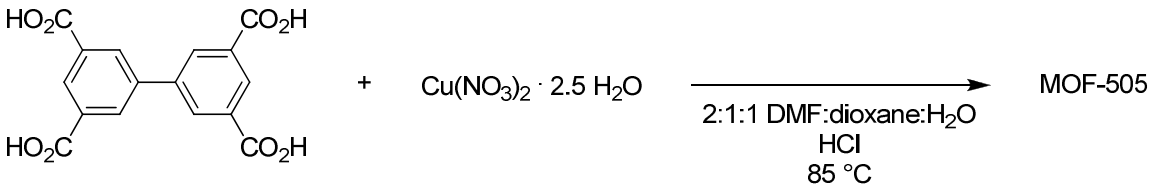

Scheme 1.4. Synthesis of MOF-505.

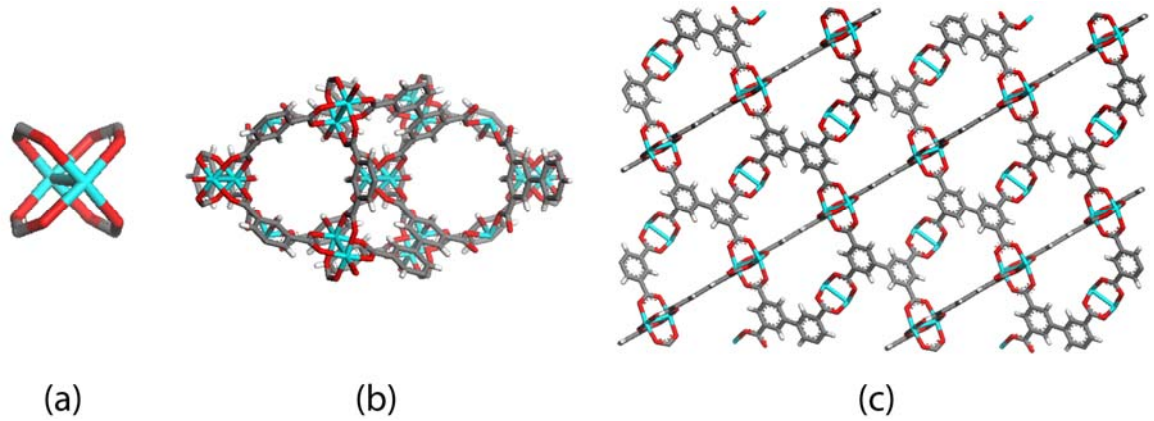

Figure 1.4. Crystal structure of MOF-505. (a) Copper paddlewheel metal cluster, (b) view of MOF-505 channels, and (c) the extended structure of MOF-505. C atoms (dark gray), H atoms (white), O atoms (red), Cu atoms (blue).

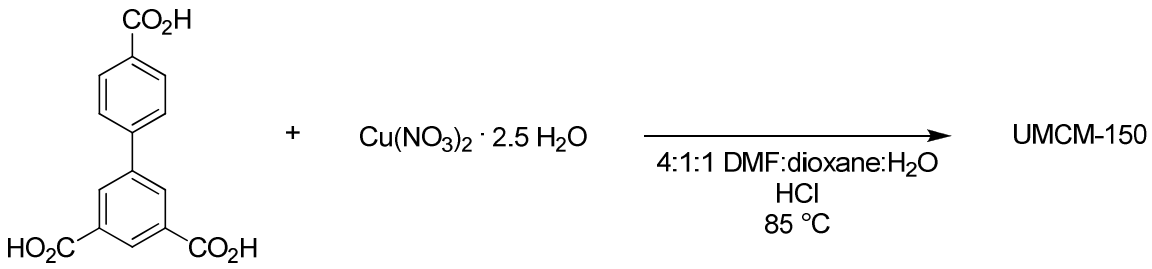

Scheme 1.5. Synthesis of UMCM-150.

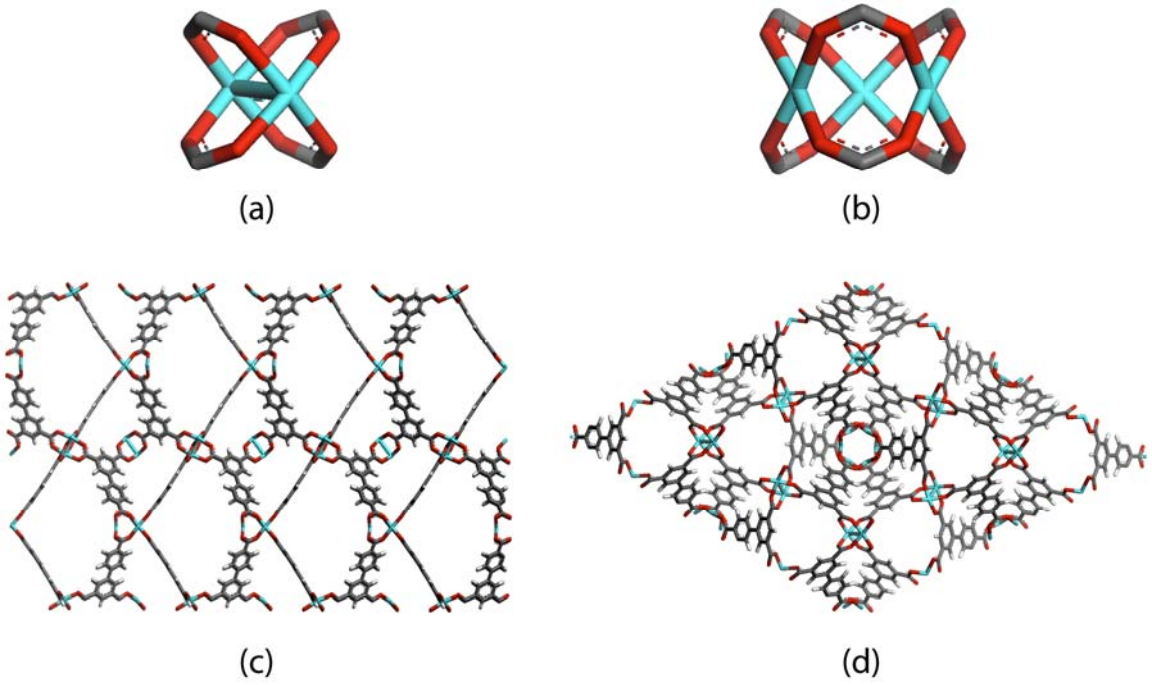

Figure 1.5. Crystal structure of UMCM-150. (a) Copper paddlewheel metal cluster, (b) trinuclear copper cluster, (c) the extended structure of UMCM-150, and (d) view of the channels in UMCM-150. C atoms (dark gray), H atoms (white), O atoms (red), Cu atoms (blue).

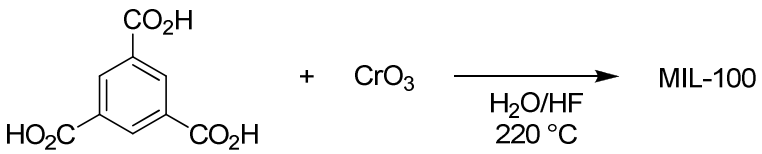

Scheme 1.6. Synthesis of MIL-100.

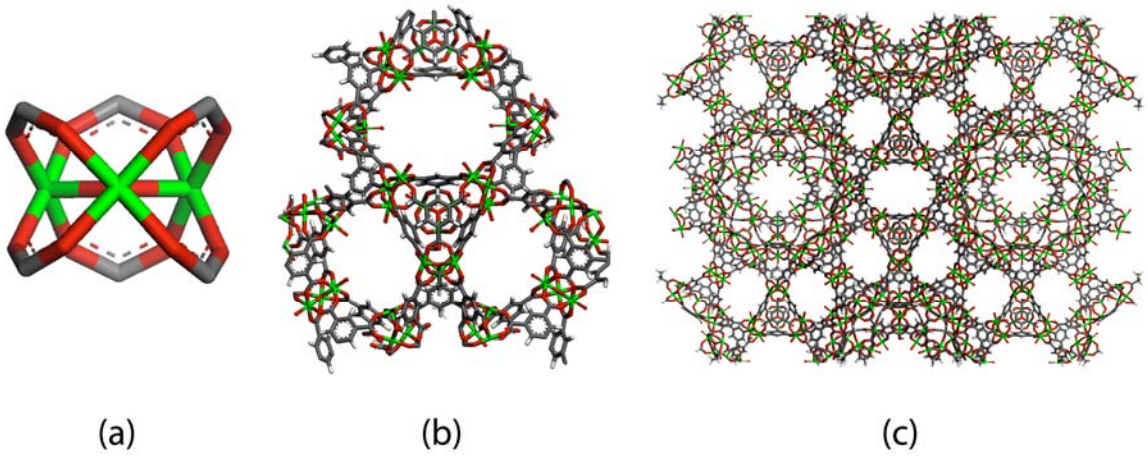

Figure 1.6. Crystal structure of MIL-100. (a) Trinuclear chromium metal cluster, (b) view of MIL-100 channels, and (c) the extended structure of MIL-100. C atoms (dark gray), H atoms (white), O atoms (red), Cr atoms (green).

Anions

Alcohols

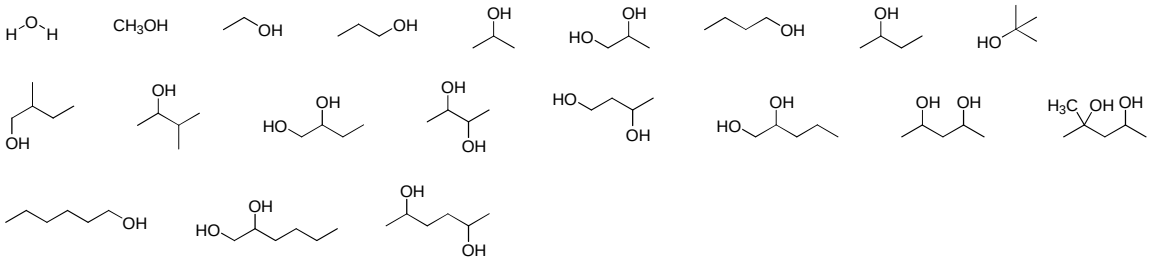

Amines

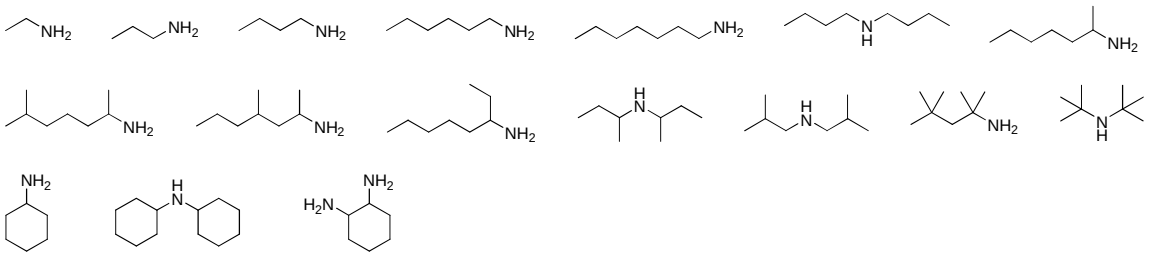

Aromatics

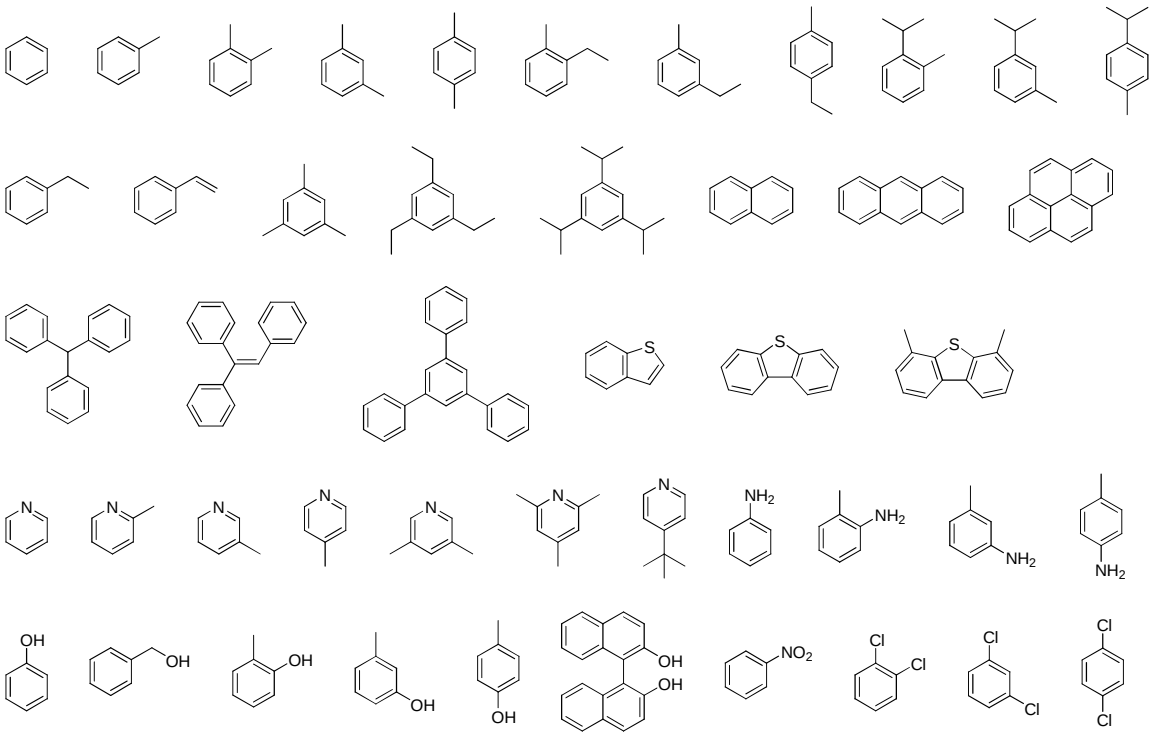

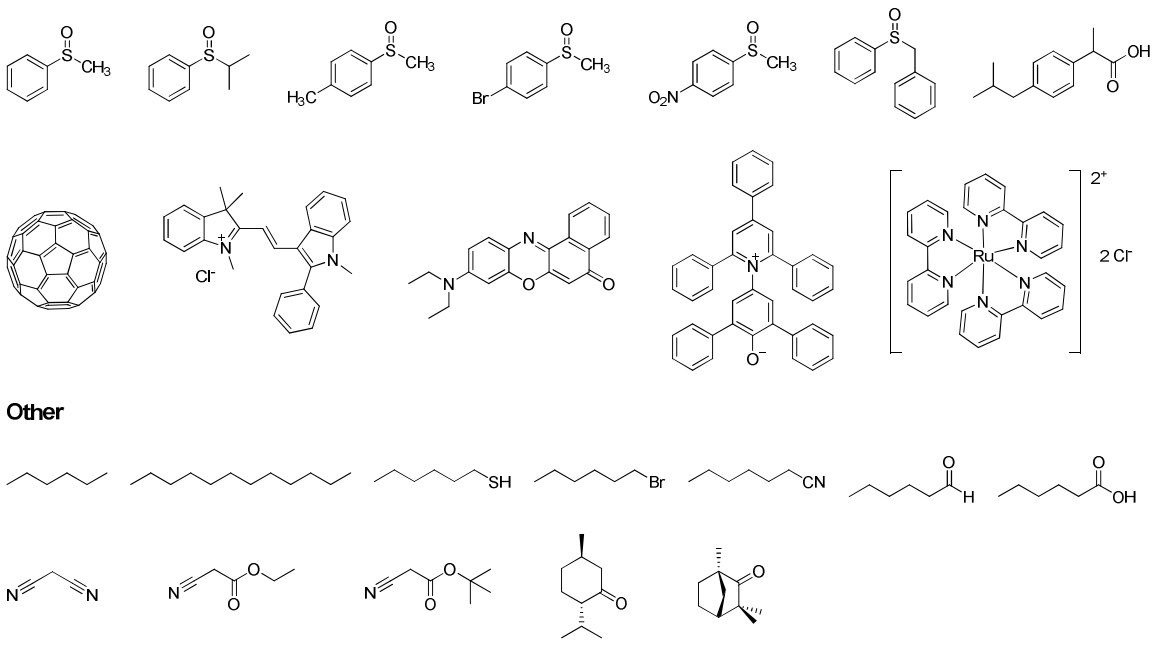

Figure 1.7. Analytes studied in liquid phase separations using MCPs.

1.5. References

(1) Deng, S. Sorbent Technology. In *Encyclopedia of Chemical Processing*; Lee, S., Ed.; Taylor & Francis Group: New York, NY, 2006; Vol. 5.

(2) Koh, K.; Wong-Foy, A. G.; Matzger, A. J. *J. Am. Chem. Soc.* **2009**, *131*, 4184-4185.

(3) Li, H.; Eddaoudi, M.; O'Keeffe, M.; Yaghi, O. M. *Nature* **1999**, *402*, 276-279.

(4) Kaye, S. S.; Dailly, A.; Yaghi, O. M.; Long, J. R. *J. Am. Chem. Soc.* **2007**, *129*, 14176-14177.

(5) Chui, S. S. Y.; Lo, S. M. F.; Charmant, J. P. H.; Orpen, A. G.; Williams, I. D. *Science* **1999**, *283*, 1148-1150.

(6) Wong-Foy, A. G.; Matzger, A. J.; Yaghi, O. M. *J. Am. Chem. Soc.* **2006**, *128*, 3494-3495.

(7) Chae, H. K.; Siberio-Pérez, D. Y.; Kim, J.; Go, Y.; Eddaoudi, M.; Matzger, A. J.; O'Keeffe, M.; Yaghi, O. M. *Nature* **2004**, *427*, 523-527.

(8) Chen, B. L.; Ockwig, N. W.; Millward, A. R.; Contreras, D. S.; Yaghi, O. M. *Angew. Chem., Int. Ed.* **2005**, *44*, 4745-4749.

(9) Lin, X.; Jia, J. H.; Zhao, X. B.; Thomas, K. M.; Blake, A. J.; Walker, G. S.; Champness, N. R.; Hubberstey, P.; Schröder, M. *Angew. Chem., Int. Ed.* **2006**, *45*, 7358-7364.

(10) Lin, X.; Telepeni, I.; Blake, A. J.; Dailly, A.; Brown, C. M.; Simmons, J. M.; Zoppi, M.; Walker, G. S.; Thomas, K. M.; Mays, T. J.; Hubberstey, P.; Champness, N. R.; Schröder, M. *J. Am. Chem. Soc.* **2009**, *131*, 2159-2171.

(11) Wong-Foy, A. G.; Lebel, O.; Matzger, A. J. *J. Am. Chem. Soc.* **2007**, *129*, 15740-15741.

(12) Férey, G.; Serre, C.; Mellot-Draznieks, C.; Millange, F.; Surblé, S.; Dutour, J.; Margiolaki, I. *Angew. Chem., Int. Ed.* **2004**, *43*, 6296-6301.

(13) Lee, J. S.; Jhung, S. H.; Yoon, J. W.; Hwang, Y. K.; Chang, J. S. *J. Ind. Eng. Chem.* **2009**, *15*, 674-676.

(14) Llewellyn, P. L.; Bourrelly, S.; Serre, C.; Vimont, A.; Daturi, M.; Hamon, L.; De Weireld, G.; Chang, J. S.; Hong, D. Y.; Hwang, Y. K.; Jhung, S. H.; Férey, G. *Langmuir* **2008**, *24*, 7245-7250.

(15) Hamon, L.; Serre, C.; Devic, T.; Loiseau, T.; Millange, F.; Férey, G.; De Weireld, G. *J. Am. Chem. Soc.* **2009**, *131*, 8775-8777.

(16) Latroche, M.; Surblé, S.; Serre, C.; Mellot-Draznieks, C.; Llewellyn, P. L.; Lee, J. H.; Chang, J. S.; Jhung, S. H.; Férey, G. *Angew. Chem., Int. Ed.* **2006**, *45*, 8227-8231.

(17) Horcajada, P.; Serre, C.; Vallet-Regí, M.; Sebban, M.; Taulelle, F.; Férey, G. *Angew. Chem., Int. Ed.* **2006**, *45*, 5974-5978.

(18) Czaja, A. U.; Trukhan, N.; Müller, U. *Chem. Soc. Rev.* **2009**, *38*, 1284-1293.

(19) Mueller, U.; Schubert, M.; Teich, F.; Puetter, H.; Schierle-Arndt, K.; Pastré, J. *J. Mater. Chem.* **2006**, *16*, 626-636.

(20) Kosal, M. E.; Chou, J. H.; Wilson, S. R.; Suslick, K. S. *Nat. Mater.* **2002**, *1*, 118-121.

(21) Stallmach, F.; Gröger, S.; Künzel, V.; Kärger, J.; Yaghi, O. M.; Hesse, M.; Müller, U. *Angew. Chem., Int. Ed.* **2006**, *45*, 2123-2126.

(22) Barthelet, K.; Marrot, J.; Riou, D.; Férey, G. *Angew. Chem., Int. Ed.* **2002**, *41*, 281-284.

(23) Loiseau, T.; Serre, C.; Huguenard, C.; Fink, G.; Taulelle, F.; Henry, M.; Bataille, T.; Férey, G. *Chem.-Eur. J.* **2004**, *10*, 1373-1382.

(24) Alaerts, L.; Kirschhock, C. E. A.; Maes, M.; van der Veen, M. A.; Finsy, V.; Depla, A.; Martens, J. A.; Baron, G. V.; Jacobs, P. A.; Denayer, J. E. M.; De Vos, D. E. *Angew. Chem., Int. Ed.* **2007**, *46*, 4293-4297.

(25) Alaerts, L.; Maes, M.; Giebeler, L.; Jacobs, P. A.; Martens, J. A.; Denayer, J. F. M.; Kirschhock, C. E. A.; De Vos, D. E. *J. Am. Chem. Soc.* **2008**, *130*, 14170-14178.

(26) Ahmad, R.; Wong-Foy, A. G.; Matzger, A. J. *Langmuir* **2009**, *25*, 11977-11979.

(27) Wong, K. L.; Law, G. L.; Yang, Y. Y.; Wong, W. T. *Adv. Mater.* **2006**, *18*, 1051-1054.

(28) Chen, B. L.; Wang, L. B.; Zapata, F.; Qian, G. D.; Lobkovsky, E. B. *J. Am. Chem. Soc.* **2008**, *130*, 6718-6719.

(29) Li, G.; Yu, W. B.; Ni, J.; Liu, T. F.; Liu, Y.; Sheng, E. H.; Cui, Y. *Angew. Chem., Int. Ed.* **2008**, *47*, 1245-1249.

(30) Seo, J. S.; Whang, D.; Lee, H.; Jun, S. I.; Oh, J.; Jeon, Y. J.; Kim, K. *Nature* **2000**, *404*, 982-986.

(31) Bradshaw, D.; Prior, T. J.; Cussen, E. J.; Claridge, J. B.; Rosseinsky, M. J. *J. Am. Chem. Soc.* **2004**, *126*, 6106-6114.

(32) Vaidhyanathan, R.; Bradshaw, D.; Rebilly, J. N.; Barrio, J. P.; Gould, J. A.; Berry, N. G.; Rosseinsky, M. J. *Angew. Chem., Int. Ed.* **2006**, *45*, 6495-6499.

(33) Evans, O. R.; Ngo, H. L.; Lin, W. B. *J. Am. Chem. Soc.* **2001**, *123*, 10395-10396.

(34) Nuzhdin, A. L.; Dybtsev, D. N.; Bryliakov, K. P.; Talsi, E. P.; Fedin, V. P. *J. Am. Chem. Soc.* **2007**, *129*, 12958-12959.

(35) Cychosz, K. A.; Ahmad, R.; Matzger, A. J. *Chem. Sci.* **2010**, in press.

(36) Cychosz, K. A.; Wong-Foy, A. G.; Matzger, A. J. *J. Am. Chem. Soc.* **2008**, *130*, 6938-6939.

(37) Park, T-H.; Cychosz, K. A.; Wong-Foy, A. G.; Matzger, A. J. *in preparation*.

(38) Cychosz, K. A.; Wong-Foy, A. G.; Matzger, A. J. *J. Am. Chem. Soc.* **2009**, *131*, 14538-14543.

CHAPTER 2

Organosulfur Compound Removal from Liquids: Equilibrium Adsorption

2.1. Introduction

As the world waits for viable clean energy solutions for the transportation sector, consumption of petroleum continues to rise dramatically. Pollution from combustion of gasoline and diesel can be broadly categorized into the inevitable (CO_2) and the byproducts arising from impurities in the hydrocarbons and/or undesired combustion byproducts (SO_x, NO_x, particulate matter). Although CO_2 capture from point sources may be feasible, there does not seem to be an actionable plan for capture from mobile sources resulting instead in a focus on reducing the other class of pollutants. The need for "cleaner" transportation fuels is recognized by increasingly stringent U.S. Department of Transportation regulations. In particular, sulfur in fuels poisons the catalysts that are necessary to remove pollutants such as nitrogen oxides (NO_x) and particulate matter from combusted fuels. This is particularly relevant for diesel, as it is responsible for much of the emissions from the transportation sector. Currently, ultra-low sulfur diesel (ULSD), with sulfur concentrations of 15 ppmw, is mandated for use in diesel vehicles – a significant reduction from 500 ppmw S low sulfur diesel that was available until 2006 Department of Transportation regulations.[1] With ULSD, diesel engines can now be designed with advanced emissions control devices to more effectively remove the

pollutants before they enter the atmosphere. According to the EPA, the new fuel standards for diesel will reduce NO_x emissions by 2.6 million tons a year and particulate matter by 110,000 tons a year.[2]

The move to ULSD has proven challenging for refineries because large organosulfur compounds such as benzothiophene (BT), dibenzothiophene (DBT) and 4,6-dimethyldibenzothiophene (DMDBT) (Figure 2.1) are difficult to remove during the fuel refining process by traditional hydrodesulfurization techniques due to poor catalyst efficiency.[3] As a consequence these refractory organosulfur compounds make up a higher proportion of refined diesel because less hindered thiophenes are removed effectively by hydrodesulfurization leading to considerable challenge in further reducing sulfur concentrations to the level needed to, for example, enable on-board reforming to power hydrogen fuel cell vehicles. One alternative strategy for removal of these compounds is to adsorb them to solid phases such as zeolites[4-10] or activated carbons;[11-17] however, the capacities, adsorption kinetics, and selectivities of these materials for the organosulfur compounds have yet to make them feasible for significant use in industry.

MCPs excel at gas adsorption and capacities greatly exceeding those of activated carbons and zeolites have been reported.[18-21] Quantitative determination of adsorption of large molecules by MCPs has seen little scrutiny despite the fact that they display adequate pore size and guest exchange kinetics.[22] To address this paucity of data in the context of an important remediation challenge, the adsorption capacities of five chemically diverse MCPs were determined for BT, DBT, and DMDBT over a wide concentration range from solutions of the organosulfur compound in isooctane. MOF-5 and HKUST-1, two of the earliest examples of highly porous MCPs, were chosen as

prototypical zinc and copper materials.[23,24] MOF-177 has superior surface area and large pore size.[25] UMCM-150 represents a new class of MCPs with reduced symmetry linkers[26] and MOF-505 is a copper material constructed from a tetracarboxylic acid.[27] These MCPs possess different pore sizes, shapes, and metal clusters thus offering a test of the key factors dictating adsorption behavior.

2.2. Model Fuel

2.2.1. Adsorption from Isooctane

Adsorption isotherms (Figure 2.2) were measured out to 2000 ppmw S in isooctane for BT and DBT and to 700 ppmw S in isooctane for DMDBT (due to low solubility). These MCPs exhibit excellent capacities for the organosulfur compounds investigated at high concentrations with, for example, BT capacities (g S/kg MCP, 1500 ppmw S) of 25, 40, and 51 for HKUST-1, UMCM-150, and MOF-505; DBT capacities (g S/kg MCP, 1500 ppmw S) of 45, 83, and 39 for HKUST-1, UMCM-150, and MOF-505; and DMDBT capacities (g S/kg MCP, 600 ppmw S) of 16, 41, and 27 for HKUST-1, UMCM-150, and MOF-505. This represents uptakes of 48 wt% and 27 wt% for DBT and DMDBT in UMCM-150. Significantly, saturation has not been reached for all isotherms, indicating that these materials have the potential for even higher adsorption amounts. For comparison, capacities (g S/kg zeolite) were measured for a benchmark zeolite material, Na(Y), at 1500 ppmw S for BT and DBT and at 600 ppmw S for DMDBT and are 8, 5, and 3, respectively. Capacity at low concentrations is an equally important performance metric, and several MCPs studied operate extremely efficiently at low concentration indicating high affinity between the organosulfur compounds studied and the framework.

MOF-505 has capacities (g S/kg MCP, 25 ppmw S) of 25 and 17 for DBT and DMDBT. In comparison, Na(Y) zeolite has a DBT capacity of 1.5 g S/kg zeolite and a DMDBT capacity of 2 g S/kg zeolite both at 25 ppmw S. Attempts were made to fit the adsorption isotherms to the Langmuir equation, but in some cases the Langmuir equilibrium constant (K) was negative, indicating that the Langmuir model may not be the best model to describe this adsorption behavior in all MCPs.

2.2.2. Factors Affecting Adsorption Capacity

Typically, correlations are observed between the surface area or pore volume of an MCP and the amount of gas adsorbed. In the concentration regime studied for large organosulfur compound adsorption, neither of these correlations holds. For example, MOF-177 has the highest surface area and pore volume of these five materials (Table 2.1), but it adsorbs the least for all three organosulfur compounds. Figure 2.3 illustrates models of one molecule of dibenzothiophene in the pore of each MCP studied. DBT is in closest contact with the framework of UMCM-150 and MOF-505: two MCPs with the highest DBT affinity as evidenced by uptake at low concentrations. However, it is also important to note that upon activation UMCM-150, MOF-505, and HKUST-1 are MCPs with coordinatively unsaturated metal centers. Although π-complexation between the organosulfur compound and the metal center is unlikely on steric grounds, other interactions with these sites may be functional.

The greatest challenge for desulfurization, and an issue common to both hydrodesulfurization and adsorption processes, has been the removal of DMDBT. The sterically hindered sulfur greatly slows the rate of hydrodesulfurization. Additionally, the small pores of zeolites (as compared to most MCPs) exclude the larger DMDBT

molecule from entering (for organosulfur compound kinetic diameters see Figure 2.4). MCPs excel here; for three of the five materials studied, the DMDBT capacity is larger than for BT and DBT at 300 ppmw S. For example, UMCM-150 has capacities (g S/kg MCP, 300 ppmw S) of 14, 34, and 37 for BT, DBT, and DMDBT. Larger guests lead to increased contact with the framework. This enhances interaction leading to higher adsorption for DMDBT. However, pore size is also a factor governing the adsorption capacity for a given organosulfur compound. For example, MOF-505, the MCP with the smallest pores studied, has its largest capacity at 300 ppmw S for DBT (38 g S/kg), but the amount adsorbed drops to 27 g S/kg for DMDBT, showing that DMDBT does not fit as well into the pores. These examples illustrate that MCPs are capable of readily removing the compound most challenging to eliminate by hydrodesulfurization thus making this an excellent complementary technique for the achievement of extremely low sulfur fuels.

2.2.3. Regeneration

The regeneration of UMCM-150 was accomplished by washing the MCP with room temperature isooctane after the equilibrium adsorption experiment to desorb the adsorbed organosulfur compound. When the DBT adsorption experiment was repeated, only a minimal decrease in the adsorption capacity was observed (Figure 2.5). Adsorbent regeneration is a key factor in ultimately determining potential for use in industry and the mild conditions needed to regenerate UMCM-150 in this equilibrium experiment indicate that MCPs may be ideal candidates for adsorptive desulfurization.

2.3. Electron Deficient MCPs

Among the MCPs tested, UMCM-150 has demonstrated excellent capacity and selectivity for removing DBT and DMDBT from solution, underscoring the potential utility of MCPs with similar pore size and shape for adsorptive desulfurization. One attractive strategy to enhance the adsorption capacity of UMCM-150 for DBT and DMDBT while maintaining pore size and shape is the reversible charge-transfer complexation of these compounds by a π-acceptor.[28-30] In this context, UMCM-150 analogs constructed from linkers **2-3** (Figure 2.6) should enhance the electronic interaction between the electron-rich organosulfur compounds and the MCP framework with electron-deficient linkers. Three isostructural MCPs have been produced from the solvothermal reactions of **1-3** and $Cu(NO_3)_2 \cdot 2.5H_2O$ (UMCM-150, UMCM-150$(N)_2$, and UMCM-150$(N)_1$) and constitute a unique platform to explore, in isolation, the effect of linker electronic nature upon organosulfur compound adsorption.[31]

Figure 2.7 displays the adsorption isotherms to 2000 ppmw S for DBT and to 500 ppmw S for DMDBT (due to solubility limitations) in isooctane for UMCM-150 and its analogs. UMCM-150$(N)_2$ adsorbs more DBT than both UMCM-150 and UMCM-150$(N)_1$ over the concentration range investigated. While the latter two MCPs exhibit similar adsorption behaviors at low concentrations, the *N*-heteroaryl decorated MCPs demonstrate enhanced capacities at high concentrations when compared to UMCM-150 with, for example, DBT capacities (g S/kg MCP, 1500 ppmw S) of 102, 94, and 83 for UMCM-150$(N)_2$, UMCM-150$(N)_1$, and UMCM-150 respectively. For DMDBT, the adsorption isotherm for UMCM-150 rises quickly up to 100 ppmw S and then increases moderately. On the other hand, the DMDBT adsorption isotherms for UMCM-150$(N)_2$

and UMCM-150$(N)_1$ increase gradually with concentration, exceeding the uptake for UMCM-150 at high concentrations, with, for example, DMDBT capacities (g S/kg MCP, 300 ppmw S) of 54, 45, and 37 for UMCM-150$(N)_2$, UMCM-150$(N)_1$, and UMCM-150 respectively. Although adsorption capacity is closely correlated with MCP pore size and shape, the uptake enhancement for UMCM-150$(N)_2$ (23% for DBT at 1500 ppmw S and 46% for DMDBT at 300 ppmw S compared to UMCM-150) among the isostructural series implies that the electron deficient linker of UMCM-150$(N)_2$ augments the interaction with the electron rich organosulfur compound by means of donor-acceptor π-π interactions in the framework (Figure 2.8), leading to unparalleled refractory organosulfur compound adsorption capacities.

UMCM-150 displays a distinctive DMDBT adsorption isotherm and the local structural features in these MCPs lead to different adsorption behaviors for the large DMDBT molecule. In contrast to linkers **2** and **3**, the phenyl C-H steric interactions in linker **1** give rise to twisting between benzene rings (Figure 2.8).[26] It is postulated that this structural characteristic leads to increased interaction between DMDBT and the UMCM-150 framework at low concentrations: the methyl group of DMDBT interacts favorably with one of the trinuclear carboxylates which is sterically less hindered due to the twist of the phenyl-carboxylate bond (Figure 2.8a). It has been reported that the methyl groups of xylene isomers can interact with the carboxylates of the MIL-53 framework and the degree of this interaction governs uptake at low adsorbate concentration.[32] This methyl-carboxylate contact, however, leads to pore blockage, resulting in the modest capacity increase beyond ~100 ppmw S. Figure 2.8a depicts the proposed DMDBT molecule packing in the UMCM-150 unit cell at 300 ppmw S, where

the pores are filled with ~5 DMDBT molecules (37 g S/kg MCP). In contrast, the electron-deficient linker of UMCM-150($N)_2$ facilitates π-π interactions with the electron-rich organosulfur compound, leading to close packing in the framework. At 300 ppmw S, where there are ~8 DMDBT molecules per UMCM-150($N)_2$ unit cell (54 g S/kg MCP), the efficient π-π stacking of the framework and the adsorbate leaves space for further adsorption of DMDBT molecules (Figure 2.8b), in agreement with the continuous rise of the adsorption isotherm.

2.4. Supramolecular Isomers

In order to further explore the role of pore size and shape on adsorption capacity, two MCPs, UMCM-152 and UMCM-153, were used to adsorb DBT and DMDBT from isooctane. UMCM-152 and UMCM-153 are comprised of the same organic linker and metal clusters, leading to two materials with nearly identical surface areas, but differ in the way the metal clusters and linkers come together (Figure 2.9).[33] Adsorption isotherms were measured out to 2000 ppmw S for DBT and to 600 ppmw S for DMDBT in isooctane and are shown in Figure 2.10. These MCPs exhibit tremendous capacities for DBT and DMDBT with, for example, DBT capacities (g S/kg MCP, 1500 ppmw S) of 59 and 89 for UMCM-152 and UMCM-153 and DMDBT capacities (g S/kg MCP, 600 ppmw S) of 82 and 40 for UMCM-152 and UMCM-153. UMCM-153 adsorbs more DBT than UMCM-152 over the entire concentration range examined likely due to a better fit of DBT in the pores of UMCM-153. At low DMDBT concentrations UMCM-153 again outperforms UMCM-152. However, at higher concentrations where the uptake of UMCM-153 begins to level off, the UMCM-152 isotherm continues to rise, leading to

higher adsorption capacities at high DMDBT concentration than for UMCM-153. It is postulated that at higher DMDBT concentration the larger DMDBT molecules begin to block further uptake in the smaller UMCM-153 pores. In contrast, the larger pores of UMCM-152 can readily accommodate the DMDBT molecule in such a way as to not block the pores for further adsorption. These two supramolecular isomers constitute a unique case where the direct effects of pore size and shape can be examined and reiterate that, in fact, different pore sizes and shapes, rather than surface area, affect the equilibrium adsorption capacity for large molecules in the liquid phase.

2.5. Adsorption from Isooctane/Toluene

Removing organosulfur compounds from model hydrocarbon solutions is trivial in comparison to removing the organosulfur compounds from much more complicated fuels due to selectivity issues. To conduct an initial assessment of the effect of competition with aromatic molecules on the adsorption of the organosulfur compounds using MCPs, toluene was chosen as a representative competitive binder. Equilibrium adsorption isotherms were plotted for 85:15 (v:v) isooctane:toluene DBT and DMDBT solutions to 2000 ppmw S for DBT and to 700 ppmw S for DMDBT (due to low solubility) and are shown in Figure 2.11. In the equilibrium adsorption experiments, with the introduction of toluene, a decrease in capacity is observed for all cases in comparison to the isooctane adsorption isotherms above. However, this decrease, especially at the low concentrations that are most applicable to industry, is minimal and large capacities are still observed, particularly for MOF-505 which has DBT and DMDBT capacities of 14 and 9 g S/kg MCP at 300 ppmw S, representing uptakes of 18 and 6.5 wt% for DBT

and DMDBT, respectively. Additionally, the capacities at 300 ppmw S of MOF-177 and MOF-5 exhibit only a small decrease from the capacities in pure isooctane, demonstrating that the capacities of the two materials studied with the largest pore volumes and surface areas are less affected by the addition of toluene to the solution. Na(Y) zeolite was again tested and, for both DBT and DMDBT, removed < 1 g S/kg zeolite up to 1500 and 700 ppmw S DBT and DMDBT, respectively. Unlike the MCPs, Na(Y) offers little selectivity for the organosulfur compounds over the toluene in the solution.

2.6. Conclusions

In conclusion, MCPs can adsorb large quantities of organosulfur compounds from the liquid phase and the exceptional levels of uptake suggest that liquid phase adsorption will be an important application for this class of materials.[34] Adsorption capacity in a given MCP is determined by pore size and shape, where the interaction between the organosulfur compound and the framework plays a key role. This is solidified by the adsorption isotherms of the supramolecular isomers UMCM-152 and UMCM-153. Constructed from the same linker and metal clusters, but possessing different pore sizes and shapes, drastically different adsorption capacities for these two MCPs were obtained.

In addition to examining pore size and shape, three isostructural MCPs possessing nearly uniform surface areas from homologous biaryl tricarboxylate linkers containing phenyl, pyrimidine, and pyridine units have been used as an ideal system to probe linker effect upon organosulfur compound adsorption. More electron-deficient UMCM-150$(N)_2$ and UMCM-150$(N)_1$ have demonstrated better adsorption performance for large

organosulfur compounds than UMCM-150. These results underscore that the electronic nature and contact interactions of the aromatic linker play an important role to enhance interactions between the host MCP framework and the large guest organic molecules in the liquid phase.

Finally, adsorption studies have shown that in model solutions MCPs are selective for the organosulfur compounds over toluene. In all cases, even with competition from toluene, MCPs outperform Na(Y) zeolite indicating that there is real potential for liquid phase adsorption in MCPs to be competitive with or better than existing adsorption technologies.

2.7. Experimental Procedures

General. MOF-177,[35] MOF-5,[35] HKUST-1,[36] MOF-505,[27,37] and UMCM-150[26] were synthesized and activated according to published procedures. Benzothiophene, (97%, Acros), dibenzothiophene (99%, Acros), 4-6-dimethyldibenzothiophene (97%, Aldrich), isooctane (HPLC grade, Fisher), and toluene (ACS reagent grade, Fisher) were used as received. Na(Y) zeolite (powder) was obtained from Strem Chemicals and used as received. Sulfur concentrations were determined using a Shimadzu GC-2010 equipped with a Shimadzu SHRX5 capillary column (L = 15 m, ID = 0.25 mm) and outfitted with both a flame ionization detector (FID) and flame photometric detector (FPD). Isotherm capacities were determined using the FID detector and were calibrated using control solutions of known sulfur concentration.

2.7.1. Adsorption Isotherms

In a typical experiment, ~10, 15, and 20 mg of MCP were added to three GC vials. 500 μL of isooctane was added to each vial. Aliquots (20, 50, 100, 250, and 500 μL) of 3000 ppmw S benzothiophene or dibenzothiophene in isooctane, or 1000 ppmw S 4,6-dimethyldibenzothiophene in isooctane were added sequentially. Between aliquots, the vials were agitated on a shaker for 2 hours (benzothiophene), 3.5 hours (dibenzothiophene), or 12 hours (4,6-dimethyldibenzothiophene) and then analyzed by GC. Shaking was used instead of stirring so as not to break up the MCP crystals during the adsorption process. Equilibration times were determined for each organosulfur compound by monitoring (GC) the concentration change until no further changes in the adsorption capacity were observed.

2.7.2. Regeneration

UMCM-150 was added to a GC vial. DBT in isooctane (1 mL, 3000 ppmw S) was added to the solid. The vial was agitated on a shaker overnight. The DBT solution was removed and the UMCM-150 was rinsed with isooctane (×6) over a 24 hour period to remove adsorbed DBT. The isooctane solution was removed and the regenerated UMCM-150 was used to plot an isotherm using the batch adsorption procedure given above.

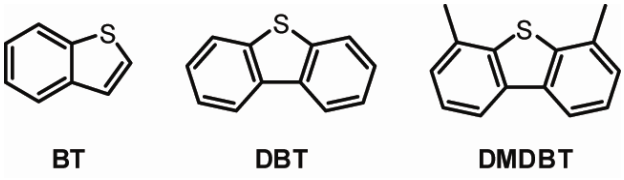

Figure 2.1. Chemical structures of benzothiophene (BT, left), dibenzothiophene (DBT, middle), and 4,6-dimethyldibenzothiophene (DMDBT, right).

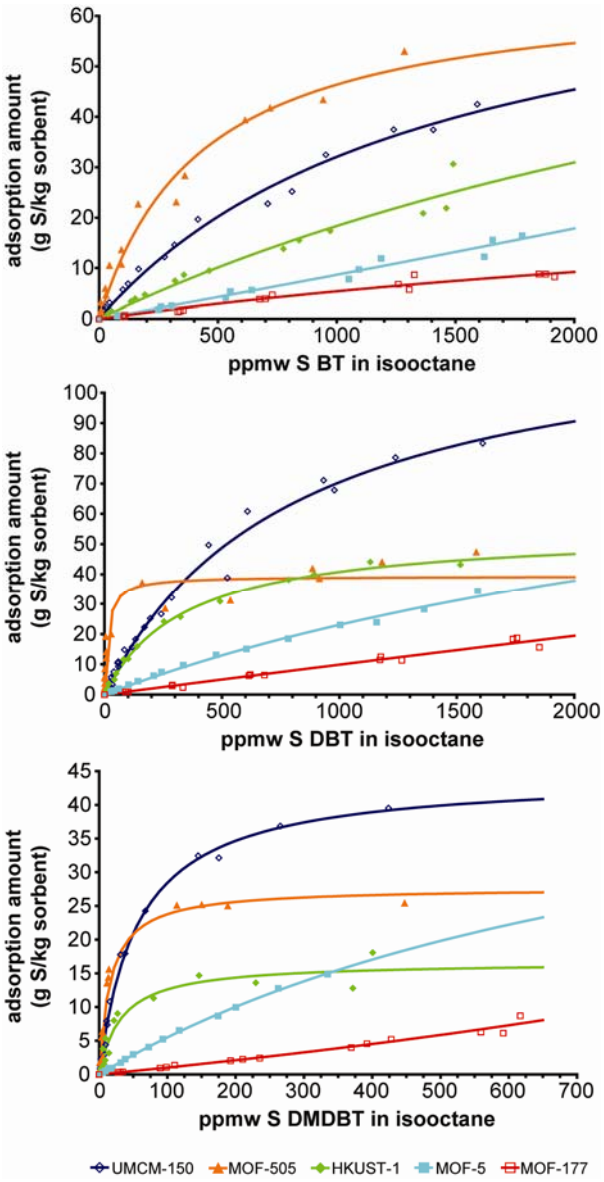

Figure 2.2. Adsorption isotherms for benzothiophene (top), dibenzothiophene (middle), and 4,6-dimethydibenzothiophene (bottom) for UMCM-150, MOF-505, HKUST-1, MOF-5, and MOF-177 from isooctane solutions. The curves represent a fit to the Langmuir equation and are intended as guides to the eye.

Table 2.1. MCP surface areas and pore volumes.

MCP	Langmuir Surface Area (m^2/g)	Pore Volume (cm^3/g)[a]
UMCM-150	3100[b]	1.11
MOF-505	1830[c]	0.71
HKUST-1	2260[d]	0.79
MOF-5	4170[d]	1.31
MOF-177	5640[d]	1.86

a) Pore volumes were calculated using the SOLV routine in PLATON (v. 1.10, University of Glasgow, 2006). The default probe radius of 1.2 Å was used with grid spacing of 0.2 Å. All solvent molecules (bound and free) were removed from the structure generated from the published CIF files prior to use of the SOLV routine. For UMCM-150 and MOF-177, disorder in the structures was not removed as it did not appreciably affect the pore volume.

b) Wong-Foy, A. G.; Lebel, O.; Matzger, A. J. *J. Am. Chem. Soc.* **2007**, *129*, 15740-15741.
c) Chen, B.; Ockwig, N. W.; Millward, A. R.; Contreras, D. S.; Yaghi, O. M. *Angew. Chem., Int. Ed.* **2005**, *44*, 4745-4749.
d) Wong-Foy, A. G.; Matzger, A. J.; Yaghi, O. M. *J. Am. Chem. Soc.* **2006**, *128*, 3494-3495.

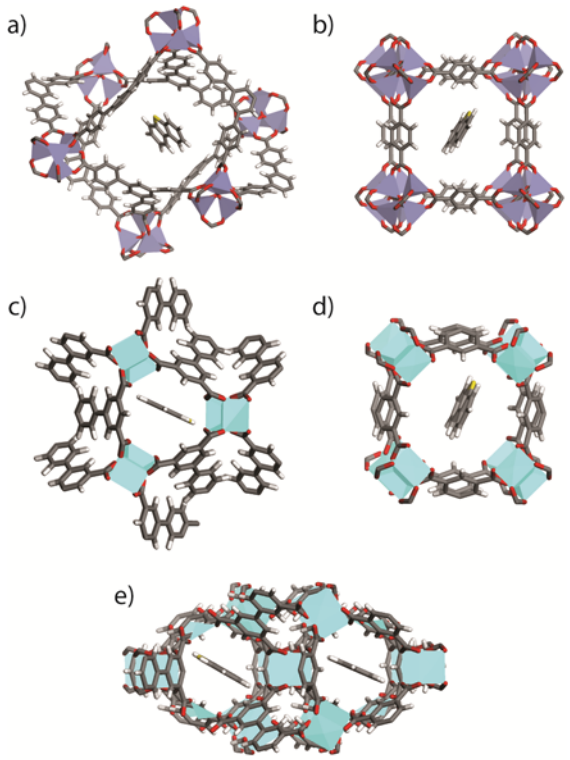

Figure 2.3. Crystal structures of (a) MOF-177 (b) MOF-5 (c) UMCM-150 (d) HKUST-1 (e) MOF-505 with one molecule of dibenzothiophene added in the pore of each MCP to represent scale.

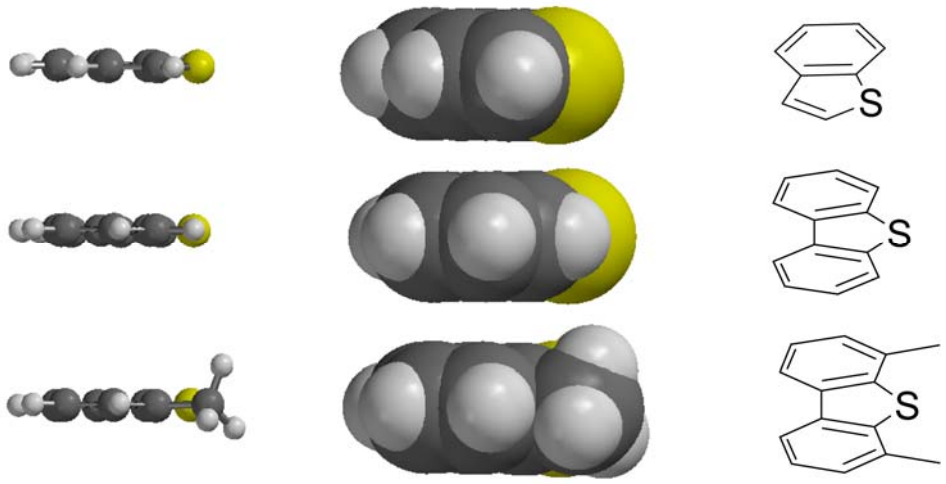

Figure 2.4. Kinetic diameters were approximated using the minimum cross-sectional area and were found to be 5.45 Å for benzothiophene (top) 5.54 Å for dibenzothiophene (middle), and 5.97 Å for 4,6-dimethyldibenzothiophene (bottom).

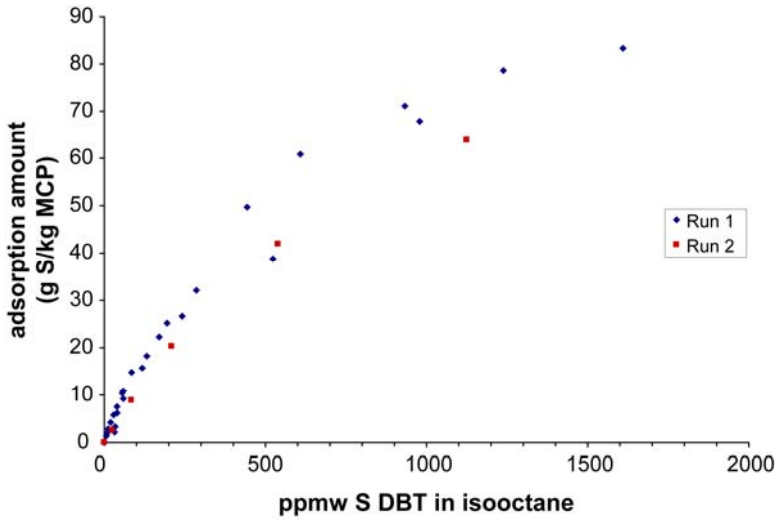

Figure 2.5. Equilibrium adsorption isotherms before and after regeneration of UMCM-150 with dibenzothiophene in isooctane. Run 1 (blue) is the initial adsorption isotherm. Run 2 (red) is after washing with room temperature isooctane.

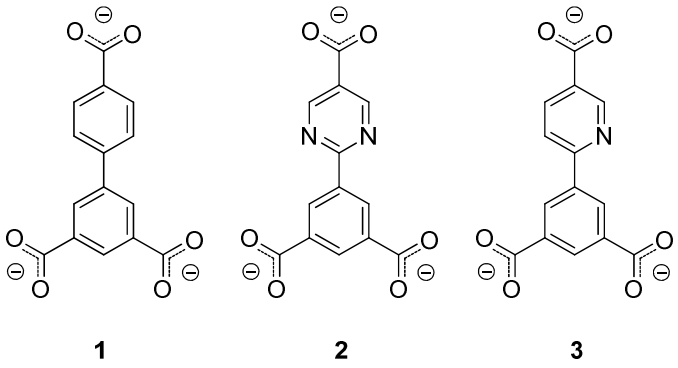

Figure 2.6. Organic ligands used to construct the isostructural MCPs UMCM-150 (**1**), UMCM-150(N)$_2$ (**2**), and UMCM-150(N)$_1$ (**3**).

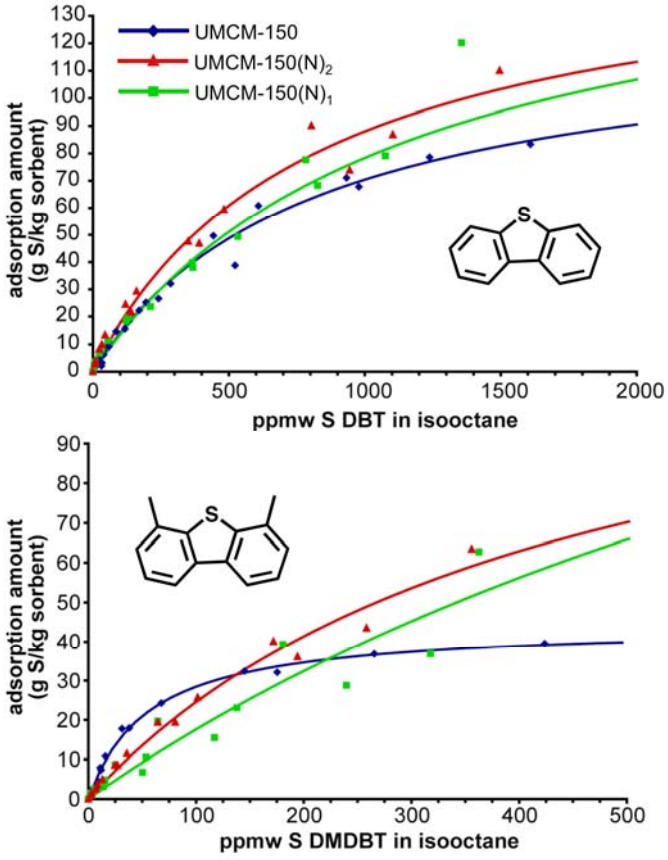

Figure 2.7. Adsorption isotherms for dibenzothiophene (top) and 4,6-dimethyldibenzothiophene (bottom) in isooctane for UMCM-150 (blue), UMCM-150(N)$_2$ (red), and UMCM-150(N)$_1$ (green). The curves represent a fit to the Langmuir equation and are intended as guides to the eye.

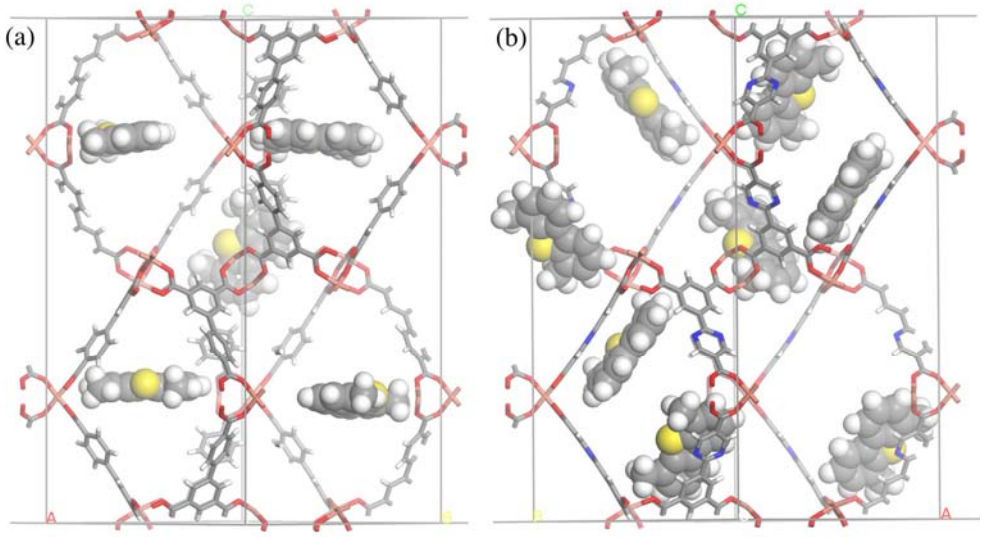

Figure 2.8. Proposed packing scheme of DMDBT molecules in (a) UMCM-150 unit cell and in (b) UMCM-150$(N)_2$ unit cell at 300 ppmw S DMDBT in isooctane.

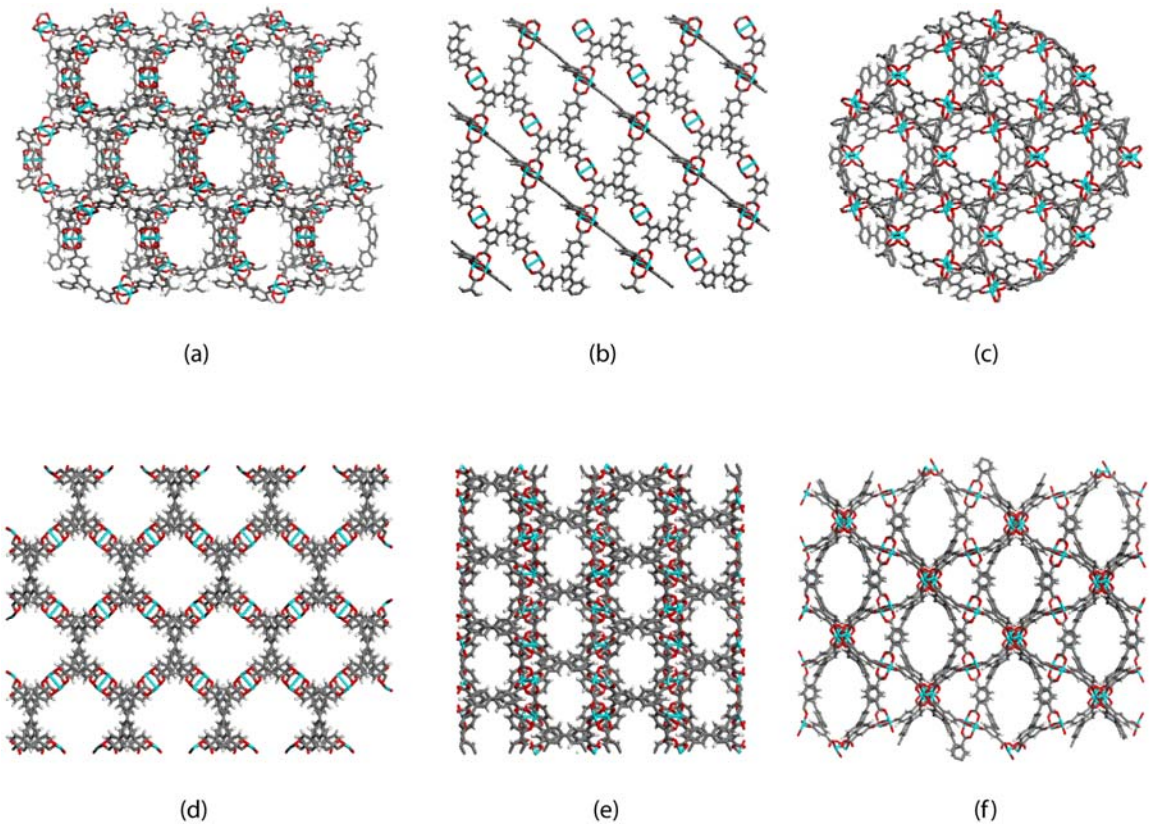

Figure 2.9. Crystal structures of UMCM-152 and UMCM-153. (a) UMCM-152, view of one of the channels, (b) UMCM-152, viewed along the b axis, (c) UMCM-152, viewed along the c axis, (d) UMCM-153, viewed along the a axis, (e) UMCM-153, viewed along the b axis, and (f) UMCM-153, view of one of the channels. C atoms (dark gray), H atoms (white), O atoms (red), and Cu atoms (blue).

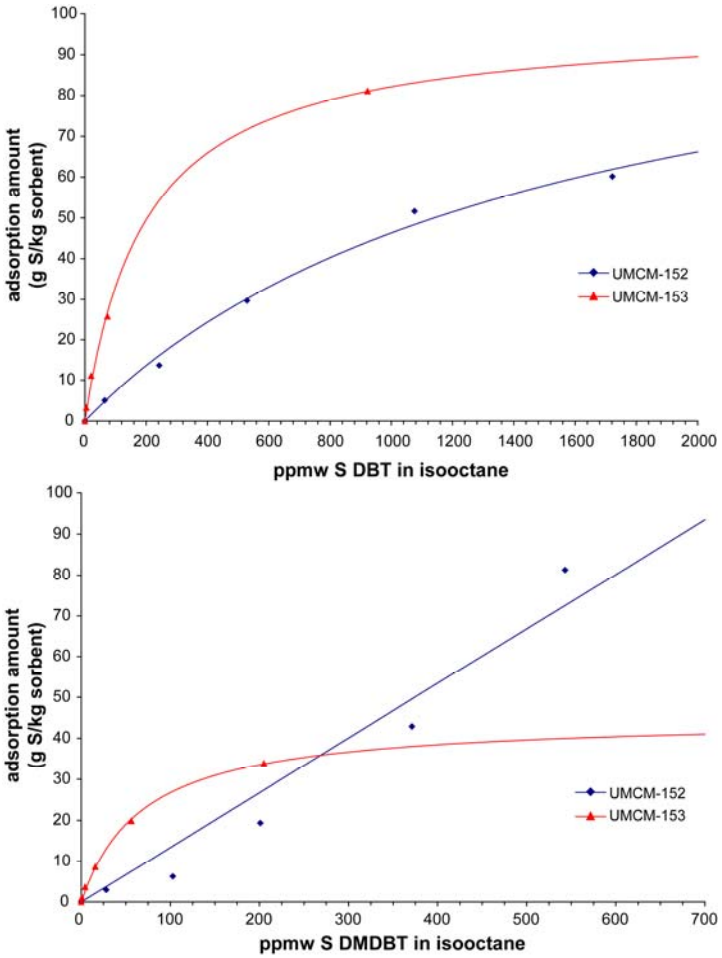

Figure 2.10. Adsorption isotherms for dibenzothiophene (top) and 4,6-dimethyldibenzothiophene (bottom) for the supramolecular isomers UMCM-152 (blue) and UMCM-153 (red). The curves represent a fit to the Langmuir equation and are intended as guides to the eye.

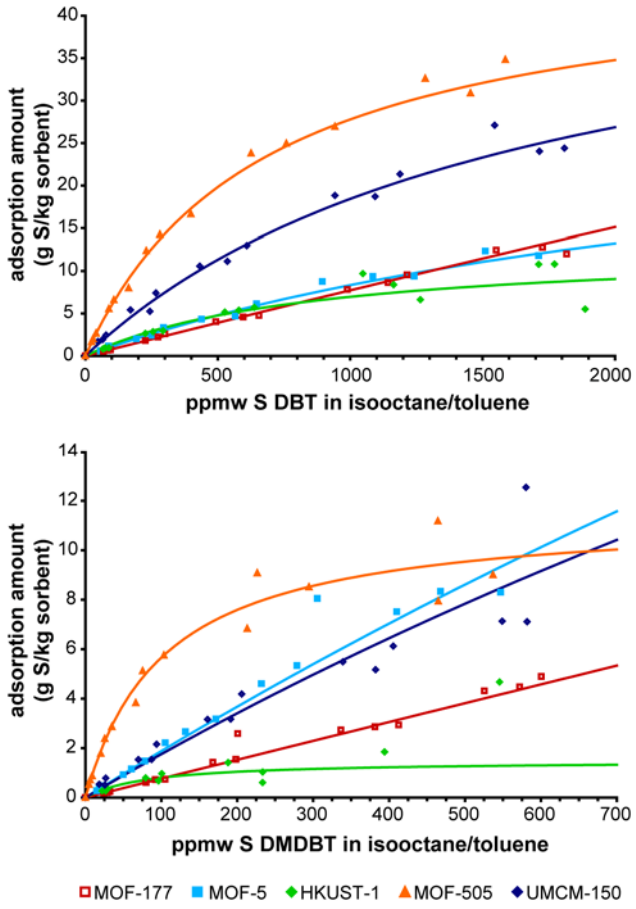

Figure 2.11. Adsorption isotherms for dibenzothiophene in 85:15 (v:v) isooctane:toluene (top) and 4,6-dimethyldibenzothiophene in 85:15 (v:v) isooctane:toluene (bottom) for MOF-177, MOF-5, HKUST-1, MOF-505, and UMCM-150. The curves represent a fit to the Langmuir equation and are intended as guides to the eye.

2.8. References

(1) *Transportation Air Quality: Selected Facts and Figures*; Publication No. FHWA-HEP-05-045; U.S. Department of Transportation: Washington, D.C., 2006.

(2) *Introduction of Cleaner-Burning Diesel Fuel Enables Advanced Pollution Control for Cars, Trucks, and Buses*; Publication No. EPA420-F-06-064; U.S. Environmental Protection Agency: Washington, D.C., 2006.

(3) Song, C.; Ma, X. L. *Appl. Catal., B* **2003**, *41*, 207-238.

(4) Hernández-Maldonado, A. J.; Yang, R. T. *J. Am. Chem. Soc.* **2004**, *126*, 992-993.

(5) King, D. L.; Faz, C. *Appl. Catal. A: Gen.* **2006**, *311*, 58-65.

(6) Ma, X. L.; Velu, S.; Kim, J. H.; Song, C. S. *Appl. Catal., B* **2005**, *56*, 137-147.

(7) Nuntang, S.; Prasassarakich, P.; Ngamcharussrivichai, C. *Ind. Eng. Chem. Res.* **2008**, *47*, 7405-7413.

(8) Velu, S.; Song, C. S.; Engelhard, M. H.; Chin, Y. H. *Ind. Eng. Chem. Res.* **2005**, *44*, 5740-5749.

(9) Weitkamp, J.; Schwark, M.; Ernst, S. *J. Chem. Soc., Chem. Commun.* **1991**, 1133-1134.

(10) Yang, R. T.; Hernández-Maldonado, A. J.; Yang, F. H. *Science* **2003**, *301*, 79-81.

(11) Ania, C. O.; Bandosz, T. J. *Langmuir* **2005**, *21*, 7752-7759.

(12) Selvavathi, V.; Chidambaram, V.; Meenalkshisundaram, A.; Sairam, B.; Sivasankar, B. *Catal. Today* **2009**, *141*, 99-102.

(13) Seredych, M.; Bandosz, T. J. *Energy Fuels* **2009**, *23*, 3737-3744.

(14) Seredych, M.; Lison, J.; Jans, U.; Bandosz, T. J. *Carbon* **2009**, *47*, 2491-2500.

(15) Yu, C.; Qiu, J. S.; Sun, Y. F.; Li, X. H.; Chen, G.; Bin Zhao, Z. *J. Porous Mat.* **2008**, *15*, 151-157.

(16) Zhou, A. N.; Ma, X. L.; Song, C. S. *J. Phys. Chem. B* **2006**, *110*, 4699-4707.

(17) Zhou, A. N.; Ma, X. L.; Song, C. S. *Appl. Catal., B* **2009**, *87*, 190-199.

(18) Kitagawa, S.; Kitaura, R.; Noro, S. *Angew. Chem., Int. Ed.* **2004**, *43*, 2334-2375.

(19) Ma, S. Q.; Sun, D. F.; Simmons, J. M.; Collier, C. D.; Yuan, D. Q.; Zhou, H. C. *J. Am. Chem. Soc.* **2008**, *130*, 1012-1016.

(20) Matsuda, R.; Kitaura, R.; Kitagawa, S.; Kubota, Y.; Belosludov, R. V.; Kobayashi, T. C.; Sakamoto, H.; Chiba, T.; Takata, M.; Kawazoe, Y.; Mita, Y. *Nature* **2005**, *436*, 238-241.

(21) Wong-Foy, A. G.; Matzger, A. J.; Yaghi, O. M. *J. Am. Chem. Soc.* **2006**, *128*, 3494-3495.

(22) Stallmach, F.; Gröger, S.; Künzel, V.; Kärger, J.; Yaghi, O. M.; Hesse, M.; Müller, U. *Angew. Chem., Int. Ed.* **2006**, *45*, 2123-2126.

(23) Chui, S. S. Y.; Lo, S. M. F.; Charmant, J. P. H.; Orpen, A. G.; Williams, I. D. *Science* **1999**, *283*, 1148-1150.

(24) Li, H.; Eddaoudi, M.; O'Keeffe, M.; Yaghi, O. M. *Nature* **1999**, *402*, 276-279.

(25) Chae, H. K.; Siberio-Pérez, D. Y.; Kim, J.; Go, Y.; Eddaoudi, M.; Matzger, A. J.; O'Keeffe, M.; Yaghi, O. M. *Nature* **2004**, *427*, 523-527.

(26) Wong-Foy, A. G.; Lebel, O.; Matzger, A. J. *J. Am. Chem. Soc.* **2007**, *129*, 15740-15741.

(27) Chen, B. L.; Ockwig, N. W.; Millward, A. R.; Contreras, D. S.; Yaghi, O. M. *Angew. Chem., Int. Ed.* **2005**, *44*, 4745-4749.

(28) Milenkovic, A.; Loffreda, D.; Schulz, E.; Chermette, H.; Lemaire, M.; Sautet, P. *Phys. Chem. Chem. Phys.* **2004**, *6*, 1169-1180.

(29) Sevignon, M.; Macaud, M.; Favre-Reguillon, A.; Schulz, J.; Rocault, M.; Faure, R.; Vrinat, M.; Lemaire, M. *Green Chem.* **2005**, *7*, 413-420.

(30) Wei, X. L.; Husson, S. M.; Mello, M.; Chinn, D. *Ind. Eng. Chem. Res.* **2008**, *47*, 4448-4454.

(31) Park, T-H.; Cychosz, K. A.; Wong-Foy, A. G.; Matzger, A. J. *in preparation*.

(32) Alaerts, L.; Maes, M.; Giebeler, L.; Jacobs, P. A.; Martens, J. A.; Denayer, J. F. M.; Kirschhock, C. E. A.; De Vos, D. E. *J. Am. Chem. Soc.* **2008**, *130*, 14170-14178.

(33) Schnobrich, J. K.; Lebel, O.; Wong-Foy, A. G.; Matzger, A. J. *in preperation*.

(34) Mueller, U.; Schubert, M.; Teich, F.; Puetter, H.; Schierle-Arndt, K.; Pastré, J. *J. Mater. Chem.* **2006**, *16*, 626-636.

(35) Millward, A. R.; Yaghi, O. M. *J. Am. Chem. Soc.* **2005**, *127*, 17998-17999.

(36) Rowsell, J. L. C.; Yaghi, O. M. *J. Am. Chem. Soc.* **2006**, *128*, 1304-1315.

(37) Lin, X.; Jia, J. H.; Zhao, X. B.; Thomas, K. M.; Blake, A. J.; Walker, G. S.; Champness, N. R.; Hubberstey, P.; Schröder, M. *Angew. Chem., Int. Ed.* **2006**, *45*, 7358-7364.

CHAPTER 3

Organosulfur Compound Removal from Liquids: Packed Bed Breakthrough Curves

3.1. Introduction

It has been previously reported that a new class of sorbents, MCPs, are well suited for the adsorption of large organosulfur compounds from model fuel solutions.[1] MCPs demonstrated extremely high capacities, exceeding those of their zeolite counterparts, in equilibrium adsorption experiments. The surface areas and pore sizes of MCPs make large molecule adsorption feasible, but the issue of selectivity has not been significantly addressed and is required to determine if a sorbent is promising for fuel desulfurization. In addition, packed bed flow-through experiments (Figure 3.1) are crucial to characterize adsorption behavior towards organosulfur compounds in an industrially relevant configuration. Unlike gas phase adsorption, liquid phase adsorption in MCPs is only beginning to be explored with few examples of liquid breakthrough in MCPs being reported.[2-5] Certainly no liquids with the complex combination of components encountered in diesel have been investigated. In addition to organosulfur compounds, fuels contain other aromatic compounds such as benzene, alkyl benzenes (e.g. toluene, xylenes), and polycyclic aromatic compounds such as naphthalenes. In total, the aromatic compounds make up around 17% of the diesel fuel, with variation depending on the

crude source of the diesel.[6] These aromatic compounds compete for adsorption sites typically leading to a decrease in the sulfur adsorption capacity of the material. This has been the case for both zeolites and activated carbons; for example, Na(Y) zeolite has been shown to favorably adsorb toluene over thiophene.[7] Furthermore, when increasing amounts of benzene are present in solution, a dramatic decrease in the DBT adsorption capacity of activated carbon has been observed.[8] MCPs may have an advantage in this regard over other adsorbents because of the ability to tailor the shape and electronics of the structure by changing the metal cluster and the organic linker to tune selectivities for the organosulfur compounds.

Packed bed breakthrough curves for the MCPs MOF-177, MOF-5, HKUST-1, MOF-505, and UMCM-150 are reported for isooctane solutions of DBT and DMDBT, the two organosulfur compounds most difficult to remove using current catalytic techniques. In order to determine the effect of aromatic compounds on adsorption capacity in MCPs, solutions of DBT and DMDBT in isooctane/toluene mixtures were tested in breakthrough experiments. To fully understand the consequence of competing aromatic molecules in the complex milieu of fuels, DBT and DMDBT in authentic diesel were also tested in breakthrough experiments.

Finally, it is extremely important that, in order for an adsorption process to be cost-effective, the packed bed can be regenerated for multiple uses. Packed beds of zeolites and activated carbons have been regenerated with varying amounts of success using combinations of heat and either gas or solvent.[9-15] Regenerability of the MCPs MOF-5 and UMCM-150 was tested under several conditions.

3.2. Breakthrough Curves from Isooctane

To benchmark the capacity of different MCPs for organosulfur compounds in the absence of competing aromatic species, packed bed breakthrough experiments were conducted with solutions of 300 ppmw S DBT in isooctane and 300 ppmw S DMDBT in isooctane. Figure 3.2 shows the resulting breakthrough curves for the five MCPs tested. These MCPs have the ability to desulfurize significant amounts of solution before the breakthrough point (defined as 1 ppmw S) with, for example, DBT breakthrough at 28, 30, and 131 mL/g MCP for MOF-505, MOF-5, and UMCM-150 and DMDBT breakthrough at 53, 23, and 92 mL/g MCP for MOF-505, MOF-5, and UMCM-150. These correspond to capacities, at breakthrough, of 5.8, 6.2, and 27.2 g S/kg MCP for DBT and 11.0, 4.8, and 19.1 g S/kg MCP for DMDBT (capacities determined by integrating above the breakthrough curve). Total capacities for these three MCPs were 20.5, 12.7, and 66.3 g S/kg MCP, respectively, for DBT and 23.8, 20.4, and 44.4 g S/kg MCP, respectively, for DMDBT; these numbers are more diagnostic for inherent materials properties than the breakthrough point because they are not subject to bed packing effects. For both organosulfur compounds, based on the breakthrough curves, UMCM-150 has the best desulfurization performance and MOF-177, the highest surface area MCP studied, is among the worst. It has been previously determined that the physicochemical parameters such as surface area and pore volume do not correlate with organosulfur compound adsorption capacity, but rather, adsorption capacity is increased with a pore size and shape that maximizes the interaction between the MCP and the organosulfur compound.[1] As a comparison, Na(Y) zeolite was also tested using the same organosulfur compound solutions. Both organosulfur compounds break through

immediately for this zeolite indicating that MCPs are favorable over this prototypical zeolite for the adsorption of DBT and DMDBT.

Current industrial desulfurization techniques such as hydrodesulfurization suffer in that the larger organosulfur compounds are more difficult to remove. Based on the breakthrough curves, MOF-505 is capable of desulfurizing more DMDBT solution before breakthrough than DBT solution, indicating that the bigger the organosulfur compound, the more successful it is at adsorbing it from solution. There have been limited examples of MCP liquid phase breakthrough curves reported in the literature,[2-5] and none for the removal of compounds as large as these organosulfur compounds, but the data presented here for the large organosulfur compounds from the liquid phase signify that MCPs are quite capable of high performance under flow-through packed bed conditions. Significantly, the liquid hourly space velocities (defined as the relationship between flow rate and bed volume) achievable with MCPs are very high due to favorable adsorption kinetics and offer conditions ideal for large scale production processes. Space velocities for MCPs used in this work are 289 hr^{-1} in comparison to typical values for zeolites of between 1 and 10 hr^{-1},[16,17] which are necessary due to diffusion limitations of the organosulfur compounds in the zeolites.[16] This result can be understood based on the much more open pore structure in MCPs offering rapid guest diffusion.[18]

3.3. Activated Carbon

Removing organosulfur compounds from model hydrocarbon solutions is trivial in comparison to removing the organosulfur compounds from much more complicated fuels due to selectivity issues. One material that illustrates this selectivity problem is

activated carbon (Figure 3.3). Activated carbon breakthrough curves were measured for both the model solution (300 ppmw S DBT in isooctane) and for spiked ultra-low sulfur diesel (ULSD, 300 ppmw S DBT in ULSD). From the breakthrough curves it is evident that, while a large capacity is seen in the aliphatic model solution, rivaling the capacities observed for MCPs, activated carbon displays virtually no selectivity for the organosulfur compound in the presence of the other components of the spiked diesel with a decrease in breakthrough point from 159 mL/g activated carbon for the isooctane solution to 13 mL/g activated carbon for the spiked diesel. This is a decrease in breakthrough capacity from 33.0 to 2.7 g S/kg activated carbon and a decrease in total capacity from 41.3 to 5.1 g S/kg activated carbon. The selectivity of activated carbon for the organosulfur compounds is very low in the presence of the other aromatic compounds in diesel.

3.4. Breakthrough Curves from Isooctane/Toluene

To assess the effect of aromatic content on organosulfur compound adsorption in packed bed experiments, breakthrough curves were plotted for 300 ppmw S DBT and DMDBT 85:15 (v:v) isooctane:toluene solutions for five MCPs (Figure 3.4). DBT breakthrough occurs at 18, 29, and 151 mL/g MCP for MOF-5, MOF-505, and UMCM-150, which corresponds to capacities at breakthrough of 3.7, 6.0, and 31.3 g S/kg MCP and overall capacities of 9.1, 14.9, and 66.6 g S/kg MCP. In comparison to the isooctane breakthrough curves shown earlier for DBT, a decrease in the breakthrough point is only seen for MOF-5 which now has a breakthrough point of 18 mL/g MCP compared to 30 mL/g MCP in the case without toluene. For the other MCPs studied, there is no decrease seen in the amount of solution that is desulfurized before the breakthrough point and

overall capacities remain similar from isooctane to isooctane/toluene. The toluene has more of an effect on the DMDBT breakthrough curves, such that DMDBT break through occurs at 15, 17, and 24 mL/g MCP for MOF-5, MOF-505, and UMCM-150, respectively, corresponding to breakthrough capacities of 3.1, 3.5, and 5.0 g S/kg MCP, which is an earlier breakthrough point for these three materials than for the isooctane solution. For the other two materials, a small increase in the amount of solution that can be desulfurized before break through is observed. Even with 15% toluene in the solution, UMCM-150 continues to outperform the other MCPs studied at breakthrough and still desulfurizes 24 mL/g MCP before sulfur breakthrough occurs. Total capacities for these three materials reach 8.0, 10.7, and 10.4 g S/kg MCP. For comparison, Na(Y) zeolite was tested using the same organosulfur compound solutions. For both DBT and DMDBT a breakthrough point of 6 mL/g MCP was observed. This is lower than the breakthrough point observed for any of the MCPs.

3.5. Breakthrough Curves from Diesel

Encouraged by the high capacity and selectivity for the organosulfur compounds over toluene, breakthrough experiments were conducted for authentic diesel solutions. ULSD was spiked to 300 ppmw S with DBT and, separately, to 300 ppmw S with DMDBT. Figure 3.5 shows the breakthrough curves for the spiked diesel solutions. The curves clearly illustrate that even in the presence of the complex mixture of aromatic compounds found in diesel MCPs are selective for the organosulfur compounds and are able to desulfurize significant amounts of fuel before the breakthrough point. For example, UMCM-150 has a breakthrough point of 70 mL/g MCP (breakthrough capacity

of 14.5 g S/kg MCP and total capacity of 25.1 g S/kg MCP) for DBT spiked diesel making it the best MCP for the flow-through packed bed removal of DBT from diesel. UMCM-150 also desulfurizes the most DMDBT spiked diesel before the breakthrough point which occurs at 52 mL/g MCP (breakthrough capacity of 10.8 g S/kg MCP and total capacity of 24.3 g S/kg MCP). Additionally, both MOF-5 and MOF-505 have breakthrough points that occur later for DMDBT than for DBT. Again, the ability to desulfurize more fuel with the larger, more sterically hindered organosulfur compound is the opposite trend observed for state-of-the-art desulfurization techniques, highlighting the advantages of adsorption to MCPs over hydrodesulfurization and adsorption to zeolites and activated carbon for the desulfurization of fuels. Comparing the MCP/spiked diesel breakthrough curves with the breakthrough curves for activated carbon (Figure 3.2), indicates that MCPs substantially outperform activated carbon. For activated carbon, a breakthrough point of 13 mL/g MCP is observed for the spiked diesel, which is earlier than for any of the MCPs tested. Additionally, the overall capacity for activated carbon (5.1 g S/kg activated carbon) is lower than the overall capacity for any of the MCPs studied.

3.6. Regeneration

To assess the ultimate utility of MCP packed beds for the desulfurization of fuels, regeneration was carried out. A packed bed of MOF-5 was fully regenerated (Figure 3.6) by flowing room temperature isooctane through the packed bed. A breakthrough curve was plotted for 300 ppmw S DBT in isooctane, regeneration was performed and the breakthrough experiment was repeated. As can be seen in the figure, there is no difference between the initial and second breakthrough curves indicating that MOF-5 is

fully regenerable under these conditions. The regeneration of a packed bed of a higher affinity material, UMCM-150, was also performed using dry toluene at 90 °C (Figure 3.7). Under these conditions, the UMCM-150 packed bed is completely regenerated with a total capacity of 72.8 g S/kg MCP for Run 1 and a total capacity of 72.4 g S/kg MCP for Run 2. The slight change in the shape of the regeneration curve from Run 1 to Run 2 likely indicates that a change in the packing of the MCP is occurring during the regeneration step. While this does not affect the overall capacity of the material, breakthrough does occur slightly earlier in Run 2 than in Run 1. Better initial packing of the MCP in the column will eliminate the discrepancy in the breakthrough curves between runs. Further proof that the organosulfur compound was completely desorbed was provided by elemental analysis which showed that, within the detection limit of 0.3%, no sulfur was present in the regenerated sample. This indicates that even the higher affinity material can be fully regenerated using only modest temperatures. However, this regeneration step has not yet been fully optimized and it is possible that alternative solvents and/or lower temperatures may also efficiently regenerate the MCP.

3.7. Conclusions

In conclusion, a uniquely complex case of liquid phase purification using MCPs has been successfully executed. The data presented demonstrate that MCPs are efficient adsorbents for fuel desulfurization. Exceptional amounts of solution are desulfurized before the breakthrough point, particularly for UMCM-150, demonstrating the utility and practicality of MCPs for this important environmental application. MCPs exhibit a selectivity for the organosulfur compounds that is not seen in other materials, such as

zeolites and activated carbon, that are also used for desulfurization. In addition, regeneration of MCP packed beds has been shown to be feasible using a combination of solvent and heat. Adsorption to MCPs is a practical way to effectively eliminate the sulfur in transportation fuels to meet the stringent current environmental standards, particularly for diesel, as well as a complementary technique to hydrodesulfurization to reduce sulfur levels in fuels to the <0.1 ppmw S necessary for fuel cell applications.

3.8. Experimental Procedures

General. MOF-177,[19] MOF-5,[19] HKUST-1,[20] MOF-505,[21,22] and UMCM-150[23] were synthesized and activated according to published procedures. Na(Y) zeolite (powder) was obtained from Strem Chemicals and activated carbon (50-200 mesh) was obtained from Fisher. Both were used as received. Dibenzothiophene (99%, Acros), 4,6-dimethyldibenzothiophene (97%, Aldrich), isooctane (HPLC grade, Fisher), and toluene (ACS reagent grade, Fisher) were used as received. Ultra-low sulfur diesel was obtained from Citgo in Ann Arbor, MI and was found to contain 32 wt% aromatic compounds using ^{1}H NMR methods[24] and 21.5 ppmw S (13.2 ppmw S dibenzothiophene and 8.3 ppmw S 4,6-dimethyldibenzothiophene) using GC-FPD. Ultra-low sulfur diesel was spiked to 300 ppmw S with DBT and DMDBT to obtain the solutions used in the experiments.

3.8.1. Breakthrough Curves

Breakthrough curves were measured by packing a stainless steel column (30 mm L × 2.1 mm ID) with the material to be studied. All packed bed experiments were performed at room temperature. The packed bed was equilibrated with isooctane at a flow

rate of 0.5 mL/min using a Hitachi L-7100 HPLC pump. A 300 ppmw S solution of the organosulfur compound was delivered at a flow rate of 0.5 mL/min. Slower flow rates were also tested, but no difference was observed in the breakthrough curve, indicating that even at 0.5 mL/min the kinetics for the adsorption of these compounds in MCPs is sufficiently favorable. The concentration of organosulfur compound in the effluent was measured using either a single wavelength UV-vis detector (Waters 486) at 330 nm for dibenzothiophene or 333 nm for 4,6-dimethyldibenzothiophene for the isooctane and isooctane/toluene solutions or a Shimadzu GC-2010 equipped with a Shimadzu SHRX5 capillary column (L = 15 m, ID = 0.25 mm) outfitted with both a flame ionization detector (FID) and a flame photometric detector (FPD) for the diesel solutions. Sulfur concentrations were determined using the FPD detector and were calibrated using solutions of known sulfur concentration. Breakthrough curves were corrected for dead volume. Total capacities were calculated by integrating above the breakthrough curve.

With the UV-vis detector, the organosulfur compound concentration exhibited non-Beer's Law behavior and correction factors were applied for each solution. To determine the correction factors, the breakthrough apparatus was equilibrated with isooctane or 85:15 (v:v) isooctane:toluene. The solution of increasing organosulfur compound concentration was delivered at a flow rate of 0.5 ml/min. The ratio of organosulfur compound solution to isooctane or 85:15 (v:v) isooctane:toluene was gradually increased from 0:100 to 10:90, 20:80, 30:70, 40:60, 50:50, 60:40, 70:30, 80:20, 90:10, and 100:0. Each concentration was allowed to equilibrate and the UV-vis absorption at 330 nm for dibenzothiophene or 333 nm for 4,6-dimethyldibenzothiophene was recorded. The process was then repeated for decreasing organosulfur compound

concentrations. The data were plotted (absorbance vs. sulfur concentration) and fit using Origin v. 7 to a sigmoidal function:

$$\text{S concentration} = (A_1 + A_2)/(1 + e^{(\text{Abs} - x)/dx}) + A_2$$

Where for dibenzothiophene in isooctane A_1 = -18.0667, A_2 = 1023.6024, x = 1.0110, dx = 0.2504; for 4,6-dimethyldibenzothiophene in isooctane A_1 = -26.4854, A_2 = 690.6192, x = 0.7824, dx = 0.2394; for dibenzothiophene in 85:15 (v:v) isooctane:toluene A_1 = -18.1995, A_2 = 991.0685, x = 1.1487, dx = 0.2874; and for 4,6-dimethyldibenzothiophene in 85:15 (v:v) isooctane:toluene A_1 = -52.3460, A_2 = 737.2321, x = 0.9420, dx = 0.3561.

3.8.2. Regeneration

Regeneration of MOF-5 packed bed was performed by flowing room temperature isooctane through the packed bed at a flow rate of 0.5 mL/min until no more organosulfur compound was eluting from the bed (as evidenced by UV-vis spectroscopy).

Regeneration of UMCM-150 packed bed was performed by flowing dry toluene through a 90 °C packed bed at a flow rate of 0.5 mL/min. The packed bed was heated using an Analytical TCM 2000 column heater. Toluene was chosen due to greater solubility of the organosulfur compounds in toluene over isooctane and elevated temperatures were necessary to efficiently remove the adsorbed dibenzothiophene.

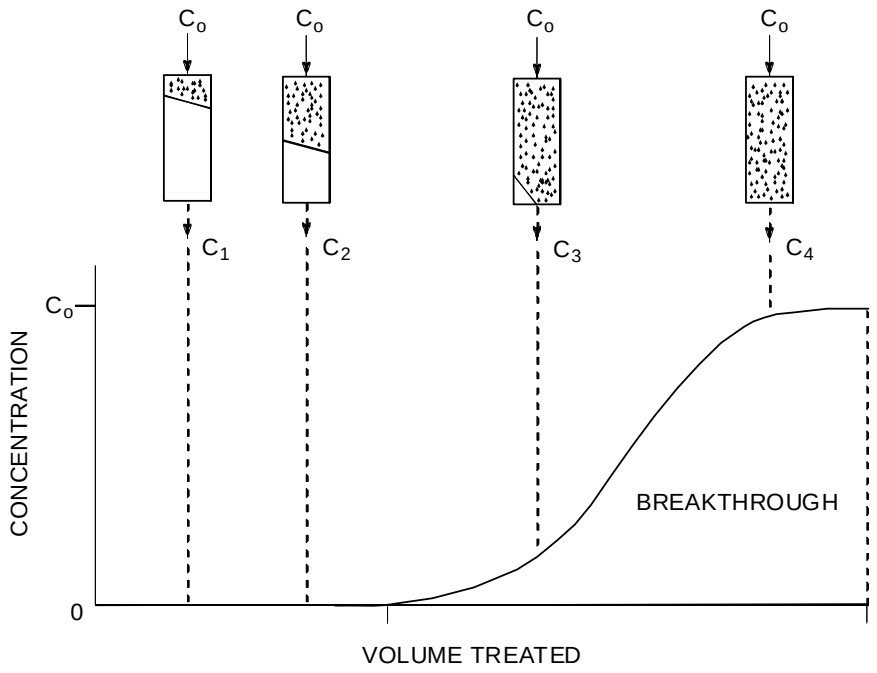

Figure 3.1. Schematic of a packed-bed breakthrough experiment. The concentration of the eluting adsorbate is monitored and plotted versus the volume of solution treated.

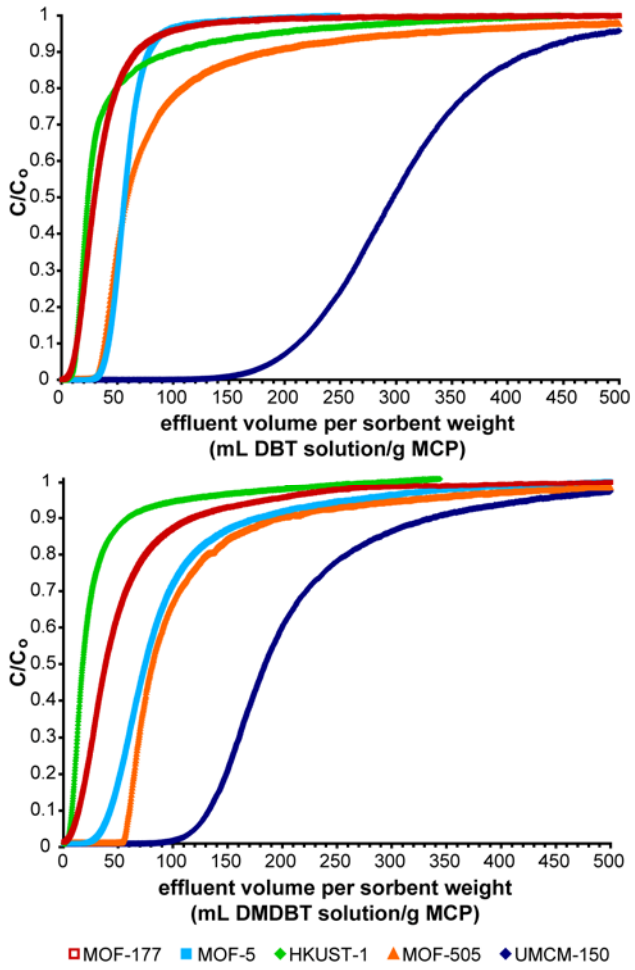

Figure 3.2. Breakthrough curves for 300 ppmw S dibenzothiophene in isooctane (top) and 300 ppmw S 4,6-dimethyldibenzothiophene in isooctane (bottom) for MOF-177, MOF-5, HKUST-1, MOF-505, and UMCM-150.

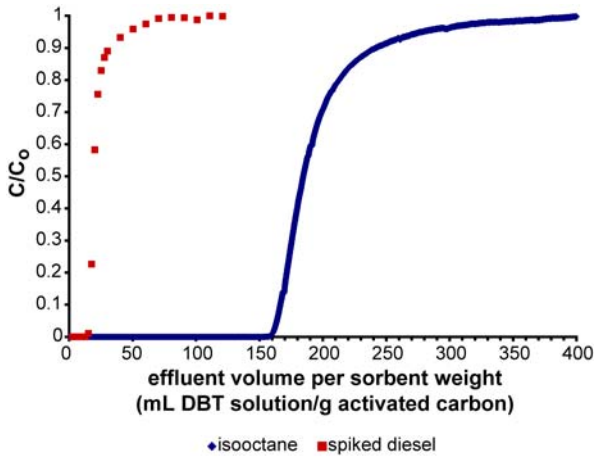

Figure 3.3. Breakthrough curves for 300 ppmw S dibenzothiophene in isooctane and 300 ppmw S dibenzothiophene in ultra-low sulfur diesel for activated carbon.

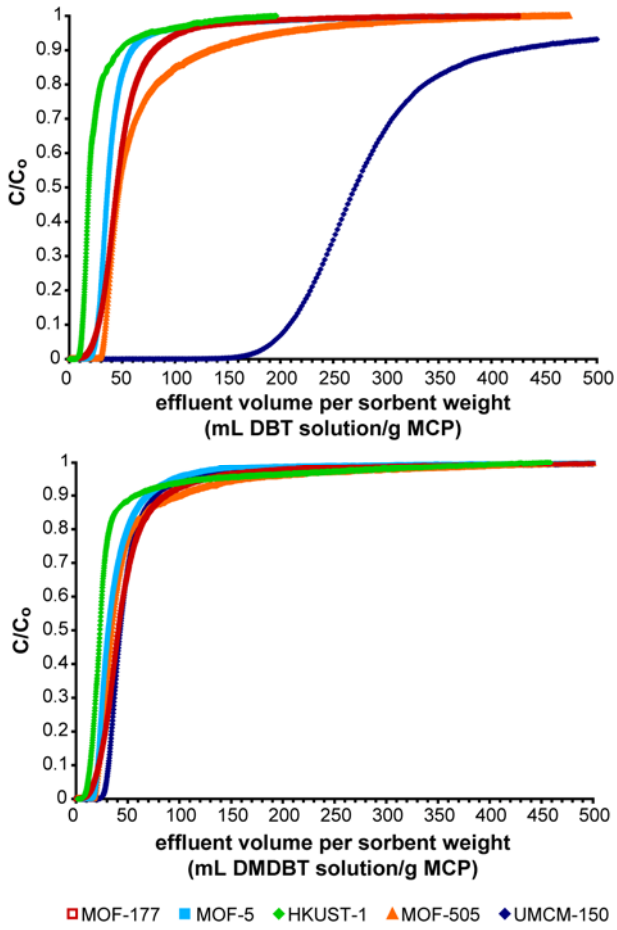

Figure 3.4. Breakthrough curves for 300 ppmw S dibenzothiophene in 85:15 (v:v) isooctane:toluene (top) and 300 ppmw S 4,6-dimethyldibenzothiophene in 85:15 (v:v) isooctane:toluene (bottom) for MOF-177, MOF-5, HKUST-1, MOF-505, and UMCM-150.

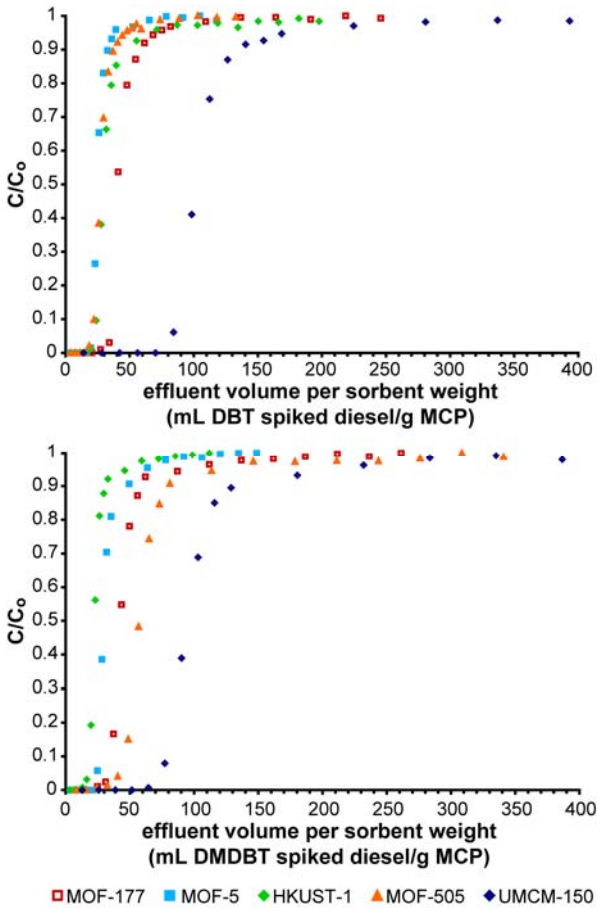

Figure 3.5. Breakthrough curves for 300 ppmw S dibenzothiophene in ultra-low sulfur diesel (top) and 300 ppmw S 4,6-dimethyldibenzothiophene in ultra-low sulfur diesel (bottom) for MOF-177, MOF-5, HKUST-1, MOF-505, and UMCM-150.

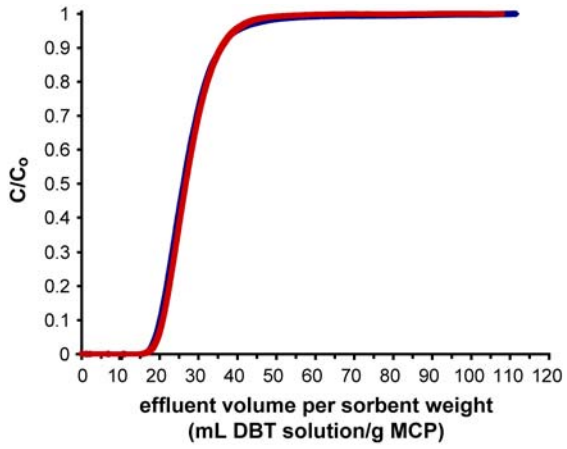

Figure 3.6. Breakthrough curves before and after regeneration of MOF-5 with dibenzothiophene in isooctane. Run 1 (blue) is the initial breakthrough curve. Run 2 (red) is after regeneration with room-temperature isooctane.

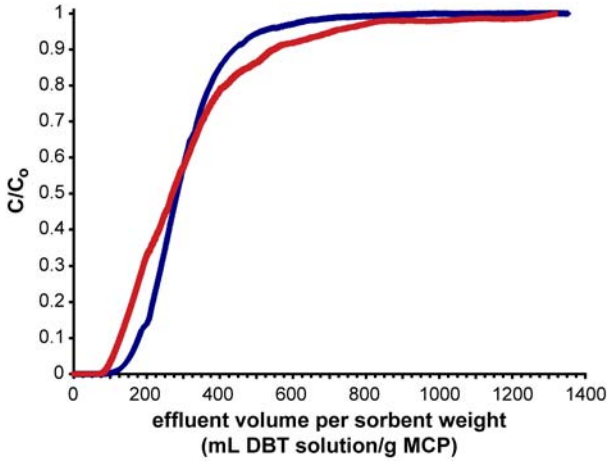

Figure 3.7. Breakthrough curves before and after regeneration of UMCM-150 with dibenzothiophene in isooctane. Run 1 (blue) is the initial breakthrough curve. Run 2 (red) is after regeneration with dry toluene at 90 °C.

3.9. References

(1) Cychosz, K. A.; Wong-Foy, A. G.; Matzger, A. J. *J. Am. Chem. Soc.* **2008**, *130*, 6938-6939.

(2) Alaerts, L.; Kirschhock, C. E. A.; Maes, M.; van der Veen, M. A.; Finsy, V.; Depla, A.; Martens, J. A.; Baron, G. V.; Jacobs, P. A.; Denayer, J. E. M.; De Vos, D. E. *Angew. Chem., Int. Ed.* **2007**, *46*, 4293-4297.

(3) Alaerts, L.; Maes, M.; Giebeler, L.; Jacobs, P. A.; Martens, J. A.; Denayer, J. F. M.; Kirschhock, C. E. A.; De Vos, D. E. *J. Am. Chem. Soc.* **2008**, *130*, 14170-14178.

(4) Alaerts, L.; Maes, M.; Jacobs, P. A.; Denayer, J. F. M.; De Vos, D. E. *Phys. Chem. Chem. Phys.* **2008**, *10*, 2979-2985.

(5) Alaerts, L.; Maes, M.; van der Veen, M. A.; Jacobs, P. A.; De Vos, D. E. *Phys. Chem. Chem. Phys.* **2009**, *11*, 2903-2911.

(6) Ma, X. L.; Sakanishi, K. Y.; Mochida, I. *Ind. Eng. Chem. Res.* **1994**, *33*, 218-222.

(7) Laborde-Boutet, C.; Joly, G.; Nicolaos, A.; Thomas, M.; Magnoux, P. *Ind. Eng. Chem. Res.* **2006**, *45*, 6758-6764.

(8) Yu, C.; Qiu, J. S.; Sun, Y. F.; Li, X. H.; Chen, G.; Bin Zhao, Z. *J. Porous Mat.* **2008**, *15*, 151-157.

(9) Hernández-Maldonado, A. J.; Stamatis, S. D.; Yang, R. T.; He, A. Z.; Cannella, W. *Ind. Eng. Chem. Res.* **2004**, *43*, 769-776.

(10) Hernández-Maldonado, A. J.; Yang, R. T. *Ind. Eng. Chem. Res.* **2003**, *42*, 123-129.

(11) Hernández-Maldonado, A. J.; Yang, R. T. *Ind. Eng. Chem. Res.* **2004**, *43*, 1081-1089.

(12) Shan, J. H.; Liu, X. Q.; Sun, L. B.; Cui, R. *Energy Fuels* **2008**, *22*, 3955-3959.

(13) Wang, Y. H.; Yang, R. T. *Langmuir* **2007**, *23*, 3825-3831.

(14) Zhang, Z. Y.; Shi, T. B.; Jia, C. Z.; Ji, W. J.; Chen, Y.; He, M. Y. *Appl. Catal., B* **2008**, *82*, 1-10.

(15) Zhou, A. N.; Ma, X. L.; Song, C. S. *J. Phys. Chem. B* **2006**, *110*, 4699-4707.

(16) Li, Y. W.; Yang, F. H.; Qi, G. S.; Yang, R. T. *Catal. Today* **2006**, *116*, 512-518.

(17) Ma, X. L.; Velu, S.; Kim, J. H.; Song, C. S. *Appl. Catal., B* **2005**, *56*, 137-147.

(18) Stallmach, F.; Gröger, S.; Künzel, V.; Kärger, J.; Yaghi, O. M.; Hesse, M.; Müller, U. *Angew. Chem., Int. Ed.* **2006**, *45*, 2123-2126.

(19) Millward, A. R.; Yaghi, O. M. *J. Am. Chem. Soc.* **2005**, *127*, 17998-17999.

(20) Rowsell, J. L. C.; Yaghi, O. M. *J. Am. Chem. Soc.* **2006**, *128*, 1304-1315.

(21) Chen, B. L.; Ockwig, N. W.; Millward, A. R.; Contreras, D. S.; Yaghi, O. M. *Angew. Chem., Int. Ed.* **2005**, *44*, 4745-4749.

(22) Lin, X.; Jia, J. H.; Zhao, X. B.; Thomas, K. M.; Blake, A. J.; Walker, G. S.; Champness, N. R.; Hubberstey, P.; Schröder, M. *Angew. Chem., Int. Ed.* **2006**, *45*, 7358-7364.

(23) Wong-Foy, A. G.; Lebel, O.; Matzger, A. J. *J. Am. Chem. Soc.* **2007**, *129*, 15740-15741.

(24) Mukherjee, S.; Kapur, G. S.; Chopra, A.; Sarpal, A. S. *Energy Fuels* **2004**, *18*, 30-36.

CHAPTER 4

Water Stability and Adsorption of Pharmaceuticals

4.1. Introduction

Water stability is an important property for any sorbent that has the potential to be used in industrial applications as moisture is usually present in at least small amounts. MCPs are traditionally viewed as being unstable to conditions where water is found as the metal-oxygen bond is easily hydrolyzed thus irreversibly destroying the structure. Recently, water stable MCPs based on imidizolate and related linkers have been synthesized.[1-3] In these cases, the greater basicity of the linker as compared to the typical carboxylic acid linkers results in stronger metal-ligand bonds and, therefore, a resistance to hydrolysis.[2] Despite the importance of the issue of water stability, there have only been limited systematic studies on the water stability of previously reported MCPs in the literature.[4,5] One combined theoretical and experimental study determined that there was a correlation between the metal cluster and the stability of the MCP upon exposure to steam, with other factors such as metal-ligand bond strength and oxidation state of the metal also playing a role in the stability.[5]

Not only is water stability important for use in industrial applications, but water stable MCPs have the potential for use in aqueous phase applications. A better understanding of the water stability in previously reported MCPs is necessary to

determine potential structures for use directly in aqueous phase applications. Other microporous materials are often used in the presence of water. For example, zeolites are common desiccants for organic solvents and activated carbons constitute the major component in tap water filtration systems. Because MCPs have been shown to outperform zeolites and activated carbons in other liquid phase adsorption applications, MCPs are prospective candidates for liquid phase applications involving water such as, for example, the removal of pharmaceutical contaminants from wastewater.

Pharmaceuticals are regarded as an emerging class of environmental contaminants and are often released directly into the environment after passing through wastewater treatment plants that are not equipped to remove them from the effluent.[6-9] Moreover, exposure of aquatic organisms to environmentally relevant concentrations of pharmaceuticals can pathologically affect the organism[10] and pharmaceuticals in water can also cause other undesirable ecological effects.[6] One strategy for removal of this class of compounds is to adsorb them to a solid phase after the traditional wastewater treatment process, but before release into the environment. Because MCPs have proven successful in liquid phase adsorption, they may be able to efficiently remove these pharmaceutical contaminants. There are only limited examples of adsorption from water using MCPs,[11-13] most likely due to the majority of MCPs being incompatible with aqueous conditions. However, water stable MCPs do exist and these structures have great potential for the treatment of wastewater.

To address the issue of water stability in MCPs, a systematic study of the effect of water concentration on the MCPs MOF-177, MOF-5, HKUST-1, MOF-505, UMCM-150, and MIL-100 has been undertaken. This diverse set of structures with differing

metal clusters and organic linkers offers insight into the factors that make a MCP water stable. Powder X-ray diffraction (PXRD) has been used to determine if the structure remains untransformed with increasing water concentration or at what water concentration the structure begins to change. Finally, HKUST-1 and MIL-100 have been tested for the adsorption of two pharmaceuticals, furosemide and sulfasalazine (Figure 4.1), from water. Furosemide and sulfasalazine were chosen in this case as representative pharmaceutical compounds that have been detected in various bodies of water throughout the world.[6,8,14-17]

4.2. Water Stability

Figures 4.2-4.7 show the PXRD patterns for as-synthesized MOF-5, MOF-177, UMCM-150, MOF-505, HKUST-1, and MIL-100, respectively, in the presence of increasing amounts of water. Changes in PXRD patterns are seen at different water:DMF ratios for each MCP studied. Interestingly, each MCP is able to exist in the presence of at least small amounts of water. MOF-5 and MOF-177, the two materials studied with basic zinc acetate metal clusters, were stable up to a water:DMF ratio of 1:4, when a change was observed in the PXRD pattern. UMCM-150 was stable up to 9:2 water:DMF, when a change was observed in the PXRD pattern for this material. Both MOF-505 and HKUST-1, comprised solely of copper paddlewheel metal clusters, were stable to ratios of 5:2 and 7:1 water:DMF, respectively. MIL-100 was stable in pure water for the one week studied. It is important to note that as-synthesized material was used for these experiments meaning that for the copper paddlewheel structures, ligands remain coordinated to the metal cluster. This may render these structures more water stable than their activated

counterparts where the coordinated ligands have been removed leaving coordinatively unsaturated metal centers.

In order to further understand the effect of water on HKUST-1, activated HKUST-1 was exposed to air for a period of 24 hours and analyzed using PXRD (Figure 4.8). No change is seen in the PXRD pattern after overnight exposure to air. Additionally, activated HKUST-1 was placed directly in water for a period of 24 hours and again analyzed using PXRD (Figure 4.9). After a period of 5 hours, no change was seen in the PXRD pattern; however, after 24 hours, although the characteristic HKUST-1 PXRD peaks remain, additional peaks are observed indicating the material is beginning to decompose and/or transform.

From this data, correlations have been observed between the metal cluster(s) in the structure and the water stability of the MCP. MOF-5 and MOF-177 both contain basic zinc acetate clusters, MOF-505 and HKUST-1 contain copper paddlewheel metal clusters, UMCM-150 contains a combination of copper paddlewheel metal clusters and trinuclear copper clusters, and MIL-100 contains trinuclear chromium clusters. MOF-5 and MOF-177 are the least stable of the MCPs studied, followed by UMCM-150, MOF-505, and HKUST-1, and finally, MIL-100 is completely water stable. Additionally, Low *et al.* have hypothesized that metal-oxygen bond strengths (estimated from common metal oxides) contribute to the water stability of an MCP.[5] CrO has a greater bond strength than CuO which has a greater bond strength than ZnO which follows in line with the water stability observed in this study. These PXRD data indicate that even MCPs such as MOF-505 and HKUST-1, which previously may have been classified as water

unstable, may still be functionable even in the presence of small amounts of water, such as that which would be found in common industrial applications.

4.3. Adsorption of Pharmaceuticals

The water stable MCP MIL-100 and the slightly water stable MCP HKUST-1 (as determined above) were chosen as adsorbents for the removal of furosemide and sulfasalazine from water. Adsorption isotherms were measured out to 0.0075 mg/mL water for furosemide and to 0.0014 mg/mL water for sulfasalazine and are shown in Figures 4.10 and 4.11 for MIL-100. In the case of both pharmaceuticals, HKUST-1 adsorbed < 1 mg/g sorbent over the entire concentration range investigated. PXRD of the HKUST-1 after the adsorption experiment showed a change in diffraction pattern comparable to those shown above for activated HKUST-1 in water. This indicates that HKUST-1 is not a suitable MCP for use in aqueous phase applications. However, MIL-100 exhibits excellent capacities for these two pharmaceuticals with a furosemide capacity of 11.8 mg furosemide/g MIL-100 at a concentration of 0.0075 mg/mL water and a sulfasalazine capacity of 6.2 mg sulfasalazine/g MIL-100 at a concentration of 0.0014 mg/mL. Additionally, PXRD of the MIL-100 after adsorption indicated no change in the structure after exposure to water. MIL-100 has the ability to remove large amounts of these compounds even at incredibly low concentrations indicating that it is a potential candidate for use in wastewater treatment. Particularly, the sulfasalazine adsorption isotherm displays a fairly steep initial rise indicating that MIL-100 is capable of adsorbing trace amounts of this compound from water, relevant for wastewater treatment effluent.

4.4. Conclusions

In conclusion, PXRD has been used to determine the water stability of a variety of MCPs. It was determined that water stability was related to the metal cluster of the MCP with structures containing basic zinc acetate metal clusters less water stable than those containing copper paddlewheel metal clusters. MIL-100, with trinuclear chromium clusters, was found to be completely water stable. This information may aid in the design of new water stable MCPs. Large adsorption capacities for the pharmaceuticals furosemide and sulfasalazine from water were obtained for MIL-100 indicating that the potential to use MIL-100 and other potentially water stable MCPs in the aqueous phase is great. Water stable MCPs are attractive alternatives for other aqueous phase adsorption applications where they have the possibility to be better than the zeolites and activated carbons that are most often used for those purposes.

4.5. Experimental Procedures

General. MOF-177,[18] MOF-5,[18] HKUST-1,[19] MOF-505,[20,21] UMCM-150,[22] and MIL-100[23] were synthesized and activated according to published procedures. Furosemide (ICN Biomedicals Inc.) and sulfasalazine (98%, Sigma-Aldrich) were used as received. Pharmaceutical concentrations were determined using an Agilent Technologies 8453 UV-visible spectrometer at room temperature and were calibrated using control solutions of known pharmaceutical concentration. Spectra were analyzed using the UV-visible Chem Station Software version B.02.01 SP1 at 331 nm for furosemide and 359 nm for sulfasalazine.

4.5.1. Powder X-ray Diffraction

Powder X-ray diffraction patterns were collected at room temperature using a Rigaku R-axis Spider diffractometer with an image plate detector and graphite monochromated Cu-Kα radiation (1.5406 Å). Samples were mounted on a cryoloop and images were collected for three minutes while rotating the sample about the φ-axis at 10°/sec, oscillating ω between 80° and 140° at 1°/sec with χ fixed at 45°. Images were integrated from 3° to 70° with a 0.05° step size using AreaMax2[24] software. Powder patterns were processed in Jade Plus.[25]

4.5.2. Water Stability Experiments

In a typical experiment, as synthesized MCP was removed from mother liquor and placed in fresh DMF (2 mL). Aliquots of deionized water (ranging from 50.0 to 2000 μL) were added to the solution sequentially. Between aliquots, the mixture was agitated at room temperature on a shaker for 1 hour and then a small amount of the solid was transferred to mineral oil and analyzed using powder X-ray diffraction.

Activated HKUST-1 was placed in a vial and deionized water (1.0 mL) was added to the vial. The mixture was agitated at room temperature on a shaker and then analyzed using powder X-ray diffraction.

Activated HKUST-1 was placed in a vial. The vial was left open to room temperature air and the sample was analyzed using powder X-ray diffraction.

4.5.3. Adsorption Isotherms

In a typical experiment, ~5 mg of MCP was added to eight GC vials. Deionized water (1 mL) was added to each vial. Aliquots (20.0, 50.0, 100.0, 250, 500, 1000, 2000, and 3000 μL) of 0.0301 mg/mL furosemide in deionized water or 0.0123 mg/mL

sulfasalazine in deionized water were added, one to each GC vial. The vials were agitated at room temperature on a shaker for 24 hours, the MCP was filtered out, and the samples were analyzed by UV-visible spectroscopy.

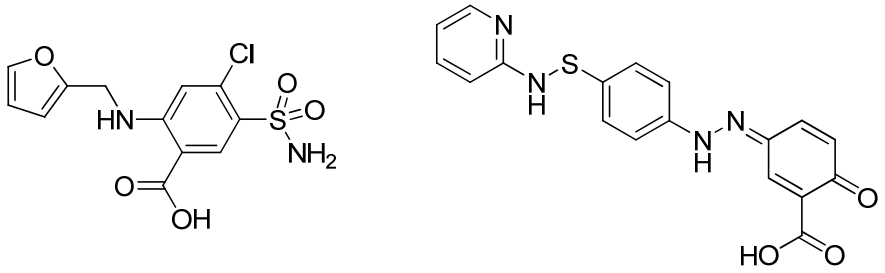

Figure 4.1. Chemical structures of furosemide (left) and sulfasalazine (right).

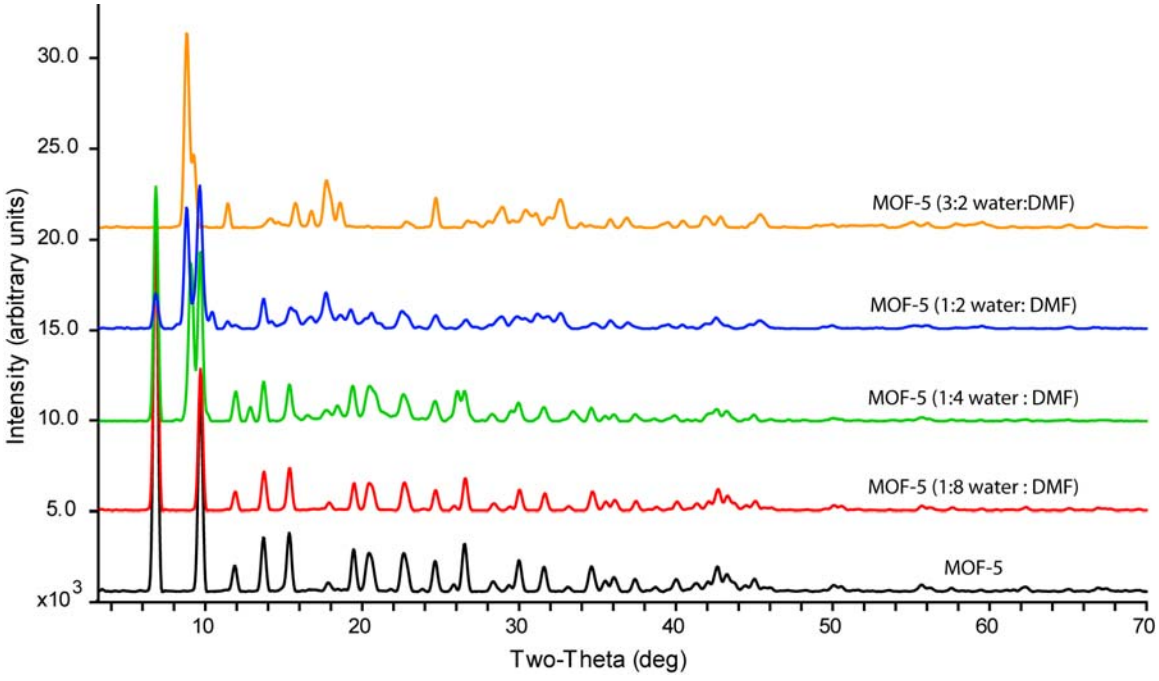

Figure 4.2. Powder X-ray diffraction patterns for MOF-5 in the presence of varying amounts of water.

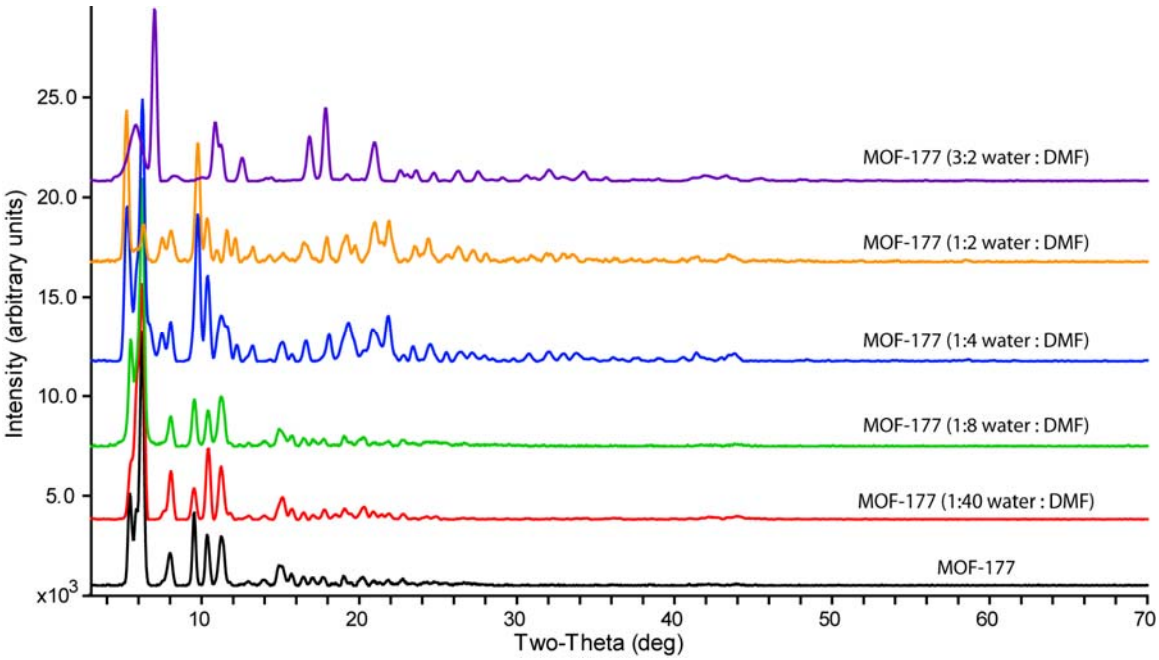

Figure 4.3. Powder X-ray diffraction patterns for MOF-177 in the presence of varying amounts of water.

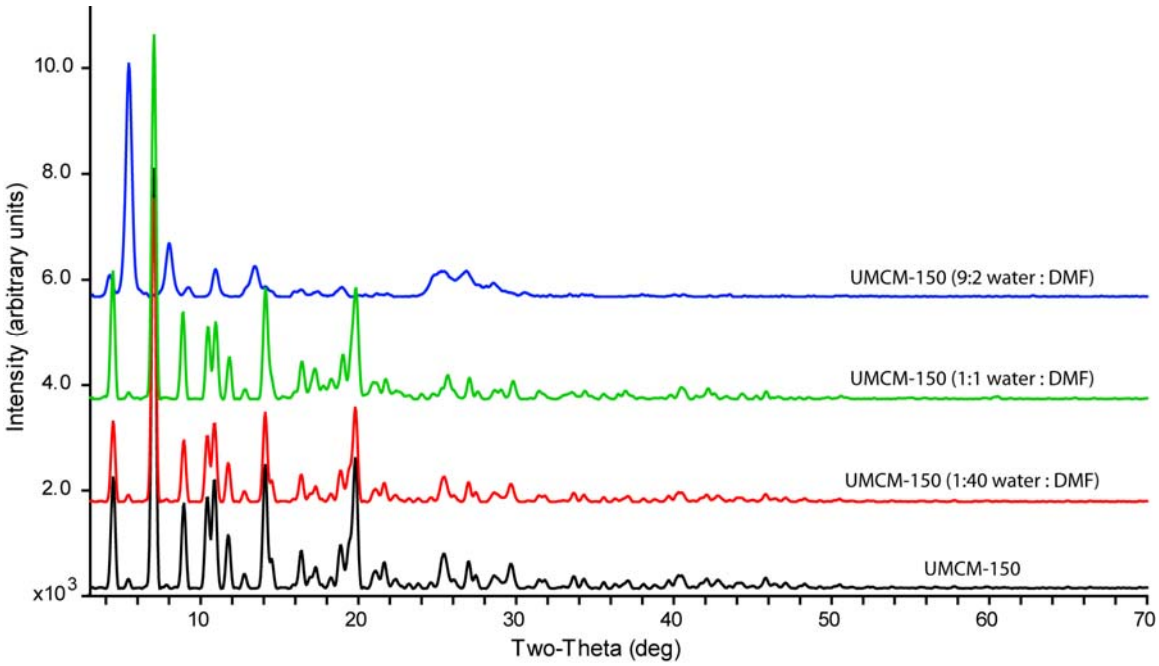

Figure 4.4. Powder X-ray diffraction patterns for UMCM-150 in the presence of varying amounts of water.

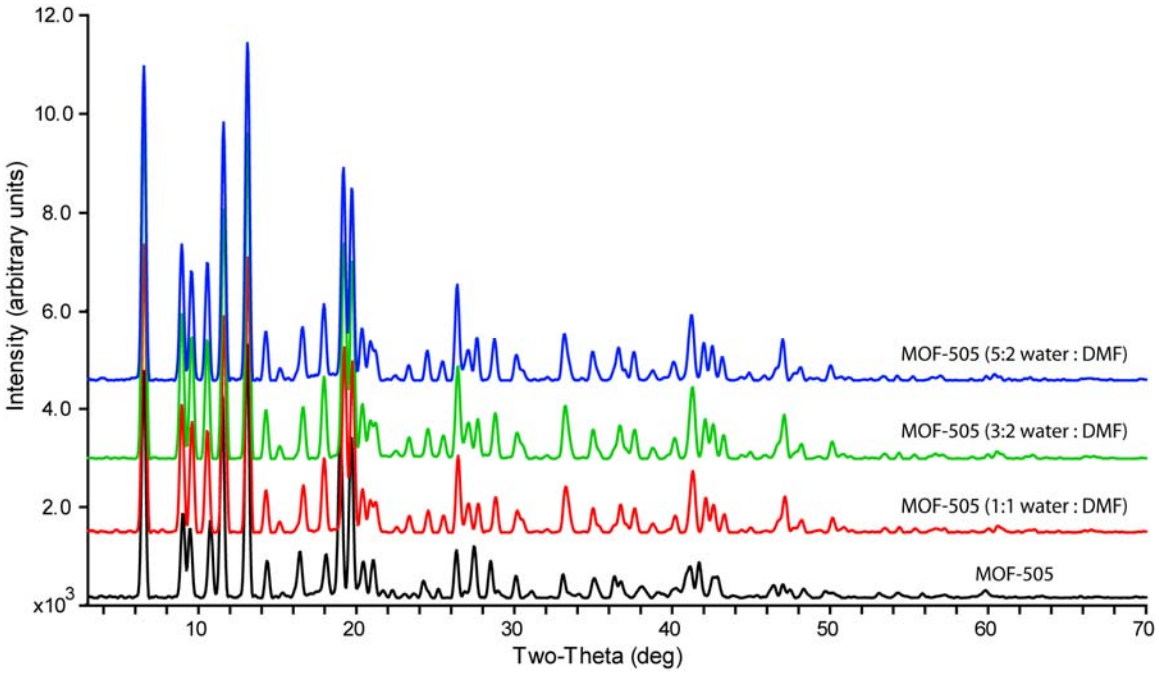

Figure 4.5. Powder X-ray diffraction patterns for MOF-505 in the presence of varying amounts of water.

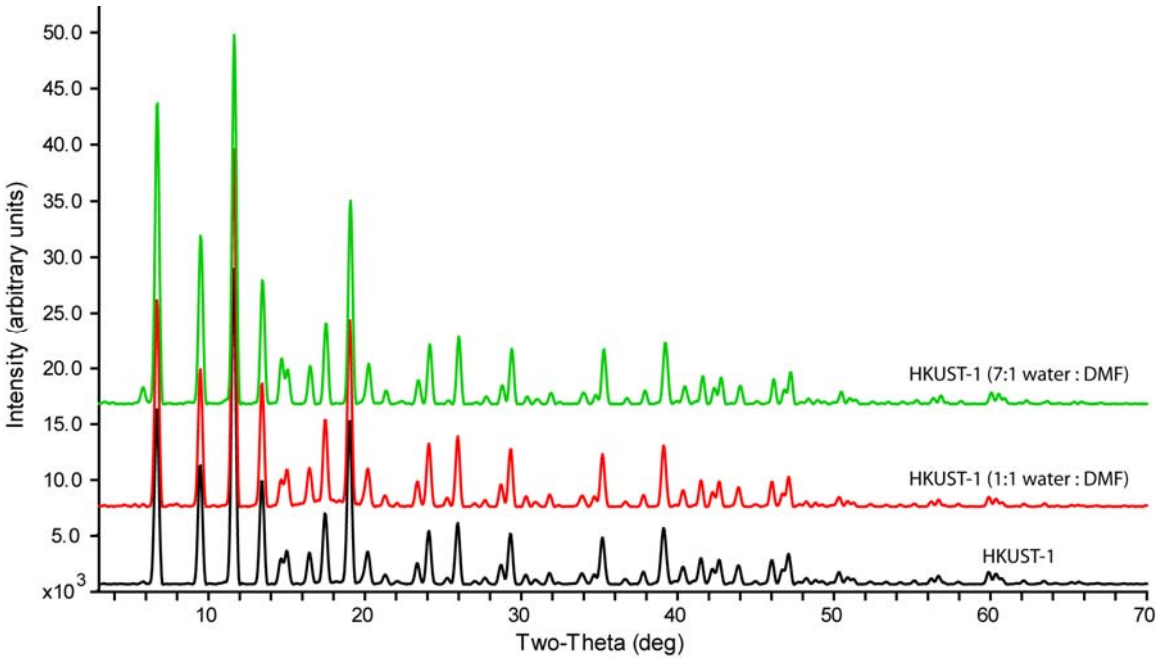

Figure 4.6. Powder X-ray diffraction patterns for HKUST-1 in the presence of varying amounts of water.

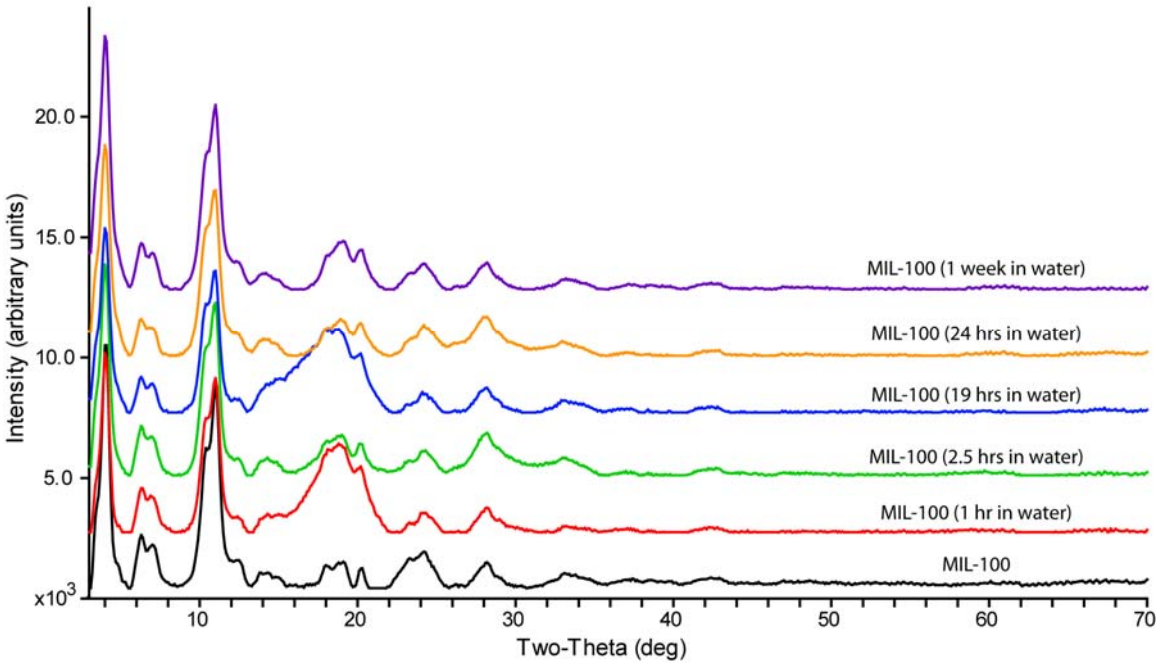

Figure 4.7. Powder X-ray diffraction patterns for MIL-100 in the presence of water.

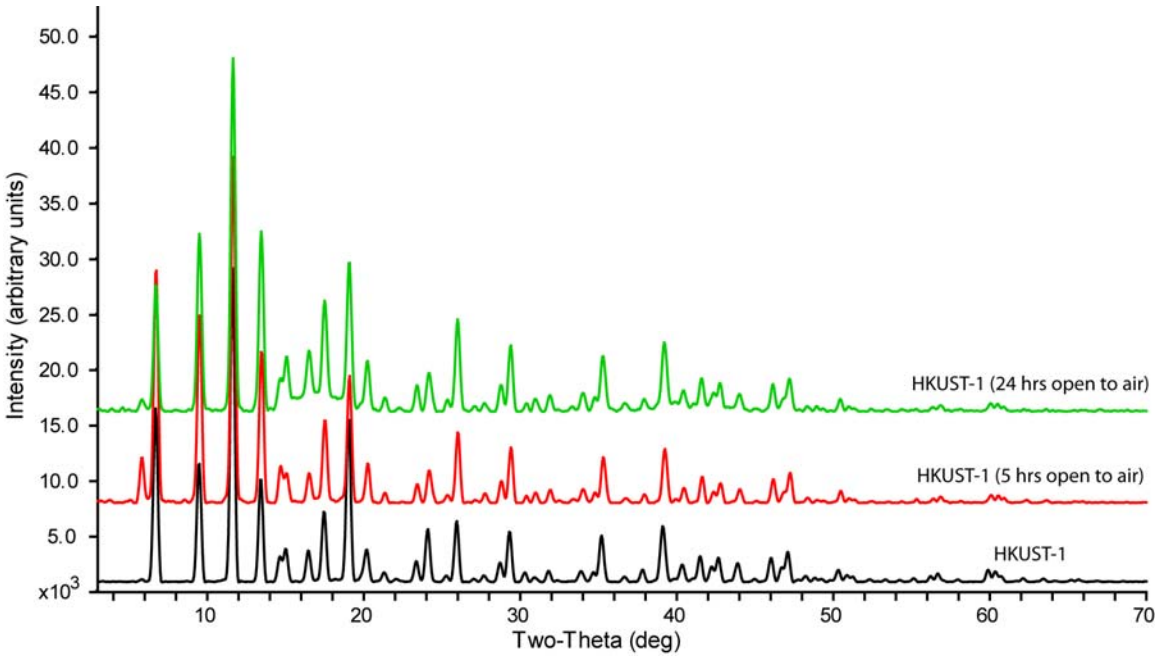

Figure 4.8. Powder X-ray diffraction patterns for evacuated HKUST-1 left open to the atmosphere.

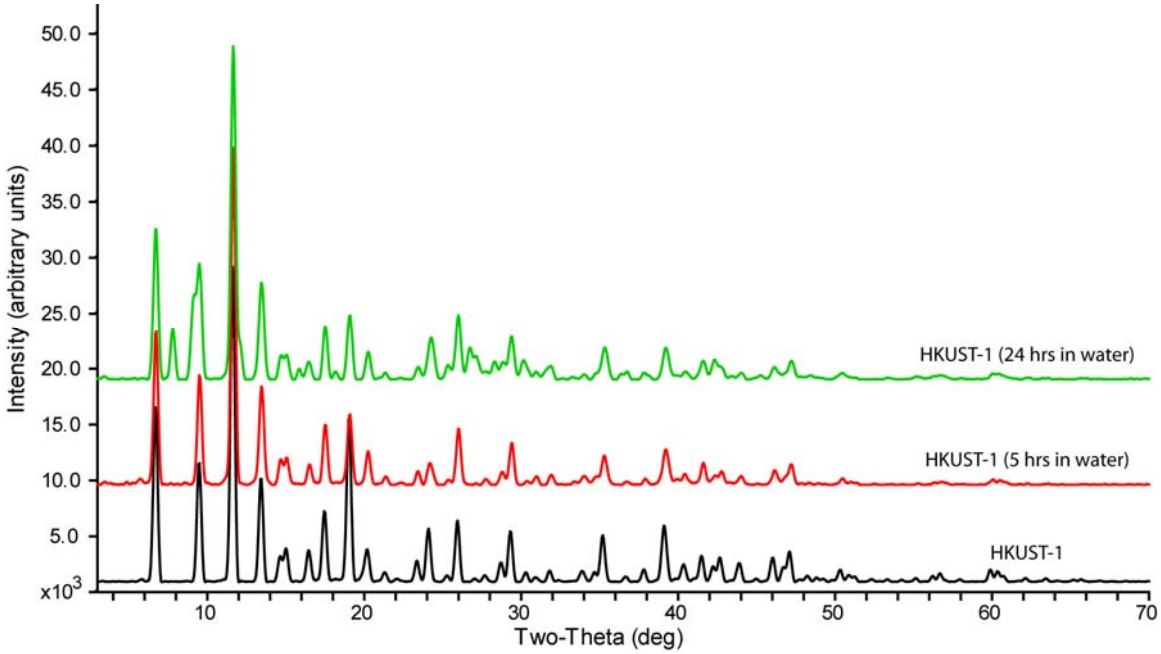

Figure 4.9. Powder X-ray diffraction patterns for evacuated HKUST-1 in water.

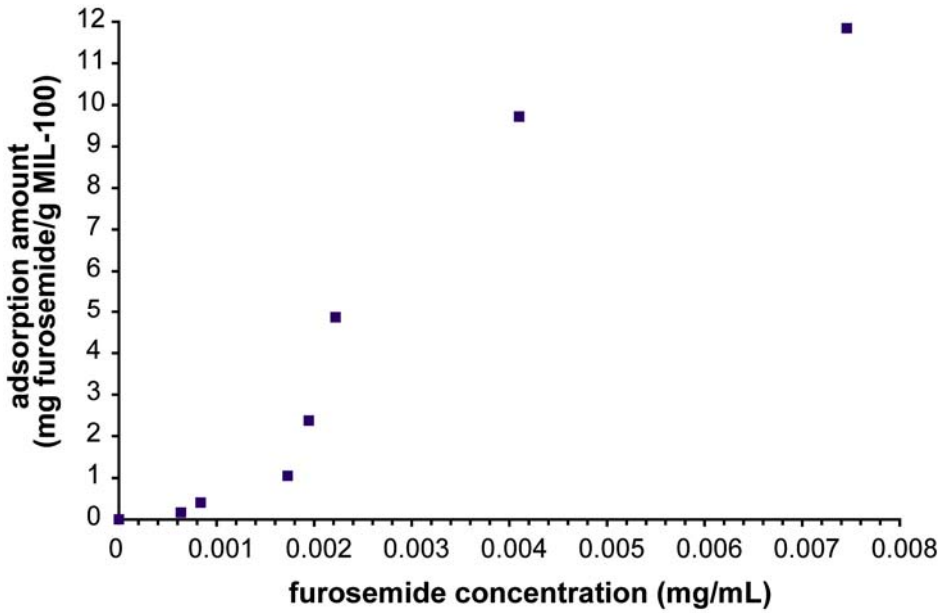

Figure 4.10. Adsorption isotherms for furosemide in water for MIL-100.

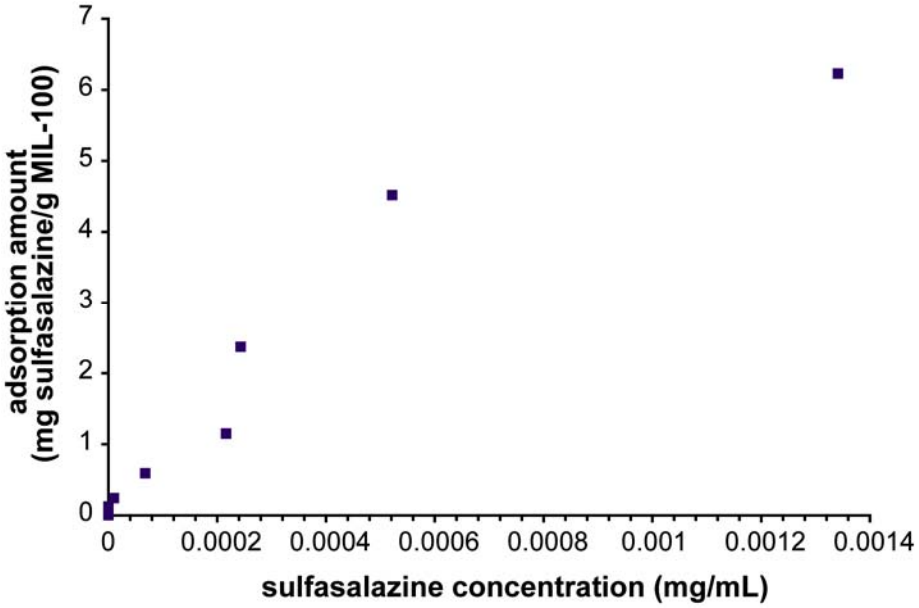

Figure 4.11. Adsorption isotherms for sulfasalazine in water for MIL-100.

4.6. References

(1) Biswas, S.; Grzywa, M.; Nayek, H. P.; Dehnen, S.; Senkovska, I.; Kaskel, S.; Volkmer, D. *Dalton Trans.* **2009**, 6487-6495.

(2) Choi, H. J.; Dincă, M.; Dailly, A.; Long, J. R. *Energy Environ. Sci.* **2010**, *3*, 117-123.

(3) Park, K. S.; Ni, Z.; Côté, A. P.; Choi, J. Y.; Huang, R. D.; Uribe-Romo, F. J.; Chae, H. K.; O'Keeffe, M.; Yaghi, O. M. *Proc. Nat. Acad. Sci.* **2006**, *103*, 10186-10191.

(4) Küsgens, P.; Rose, M.; Senkovska, I.; Fröde, H.; Henschel, A.; Siegle, S.; Kaskel, S. *Microporous Mesoporous Mat.* **2009**, *120*, 325-330.

(5) Low, J. J.; Benin, A. I.; Jakubczak, P.; Abrahamian, J. F.; Faheem, S. A.; Willis, R. R. *J. Am. Chem. Soc.* **2009**, *131*, 15834-15842.

(6) Batt, A. L.; Kostich, M. S.; Lazorchak, J. M. *Anal. Chem.* **2008**, *80*, 5021-5030.

(7) Benotti, M. J.; Trenholm, R. A.; Vanderford, B. J.; Holady, J. C.; Stanford, B. D.; Snyder, S. A. *Environ. Sci. Technol.* **2009**, *43*, 597-603.

(8) Kasprzyk-Hordern, B.; Dinsdale, R. M.; Guwy, A. J. *Water Res.* **2009**, *43*, 363-380.

(9) Kolpin, D. W.; Furlong, E. T.; Meyer, M. T.; Thurman, E. M.; Zaugg, S. D.; Barber, L. B.; Buxton, H. T. *Environ. Sci. Technol.* **2002**, *36*, 1202-1211.

(10) Kostich, M. S.; Lazorchak, J. M. *Sci. Total Environ.* **2008**, *389*, 329-339.

(11) Bai, Y.; He, G. J.; Zhao, Y. G.; Duan, C. Y.; Dang, D. B.; Meng, Q. J. *Chem. Commun.* **2006**, 1530-1532.

(12) Jhung, S. H.; Lee, J. H.; Yoon, J. W.; Serre, C.; Férey, G.; Chang, J. S. *Adv. Mater.* **2007**, *19*, 121-124.

(13) Wong, K. L.; Law, G. L.; Yang, Y. Y.; Wong, W. T. *Adv. Mater.* **2006**, *18*, 1051-1054.

(14) Balakrishnan, V. K.; Terry, K. A.; Toito, J. *J. Chromatogr. A* **2006**, *1131*, 1-10.

(15) Bueno, M. J. M.; Aguera, A.; Gómez, M. J.; Hernando, M. D.; García-Reyes, J. F.; Fernández-Alba, A. R. *Anal. Chem.* **2007**, *79*, 9372-9384.

(16) Siemens, J.; Huschek, G.; Siebe, C.; Kaupenjohann, M. *Water Res.* **2008**, *42*, 2124-2134.

(17) Stackelberg, P. E.; Furlong, E. T.; Meyer, M. T.; Zaugg, S. D.; Henderson, A. K.; Reissman, D. B. *Sci. Total Environ.* **2004**, *329*, 99-113.

(18) Millward, A. R.; Yaghi, O. M. *J. Am. Chem. Soc.* **2005**, *127*, 17998-17999.

(19) Rowsell, J. L. C.; Yaghi, O. M. *J. Am. Chem. Soc.* **2006**, *128*, 1304-1315.

(20) Chen, B. L.; Ockwig, N. W.; Millward, A. R.; Contreras, D. S.; Yaghi, O. M. *Angew. Chem., Int. Ed.* **2005**, *44*, 4745-4749.

(21) Lin, X.; Jia, J. H.; Zhao, X. B.; Thomas, K. M.; Blake, A. J.; Walker, G. S.; Champness, N. R.; Hubberstey, P.; Schröder, M. *Angew. Chem., Int. Ed.* **2006**, *45*, 7358-7364.

(22) Wong-Foy, A. G.; Lebel, O.; Matzger, A. J. *J. Am. Chem. Soc.* **2007**, *129*, 15740-15741.

(23) Llewellyn, P. L.; Bourrelly, S.; Serre, C.; Vimont, A.; Daturi, M.; Hamon, L.; De Weireld, G.; Chang, J. S.; Hong, D. Y.; Hwang, Y. K.; Jhung, S. H.; Férey, G. *Langmuir* **2008**, *24*, 7245-7250.

(24) AreaMax 2.0.0.4 ed.; Rigaku, 2005.

(25) Jade Plus 8.2 ed.; Materials Data, Inc, 1995-2007.

CHAPTER 5

Conclusions and Future Directions

5.1. Introduction

In this thesis, microporous coordination polymers were studied as adsorbents for the separation of large organic compounds (Figure 5.1) from complex matrices. In particular, MCPs were used for the desulfurization of model and diesel fuels in both equilibrium[1] and packed-bed breakthrough experiments.[2] Their organosulfur compound adsorption capabilities were compared to common sorbents such as zeolites and activated carbon and MCPs outperformed these materials in both equilibrium and packed bed breakthrough experiments. It was found that organosulfur compound adsorption capacity depends on the size and shape of the pore and that the use of electron deficient MCPs increases the capacity compared to less electron deficient analogs.[3] Additionally, MCPs were found to be selective for the organosulfur compounds over the many other components of diesel fuel. MCPs were also fully regenerated under mild conditions. Although these experiments indicate that MCPs may by ideal candidates for the desulfurization of diesel, currently, it will be challenging to choose an MCP that is cost effective to mass produce yet still exhibits high capacity and selectivity for the organosulfur compounds. To date, MCPs are often synthesized from specialized organic ligands and/or solvents making them expensive materials to produce. Additionally,

regeneration conditions still need to be optimized to find the right combination of solvent and temperature to effectively desorb the organosulfur compounds in a way that does not drive up the cost of the overall desulfurization process.

Further, MCPs have not been extensively used in aqueous applications due to their water instability. In this thesis, the water stability of common MCPs was studied via powder X-ray diffraction and a water stable MCP, MIL-100, was used to adsorb the pharmaceuticals furosemide and sulfasalazine from water. A correlation was observed between the metal cluster and the water stability of the MCP. For MIL-100, large capacities were obtained at very low pharmaceutical concentration, making MIL-100 an ideal candidate for the removal of contaminants from wastewater. The regeneration conditions required for water stable MCPs to desorb adsorbed pharmaceuticals have yet to be determined.

Here, areas of further study are discussed from those specific to the projects in this thesis to those general for advancing the study of liquid phase adsorption in MCPs: adsorption in mixed organosulfur compound systems, determination of the interaction between the MCP and the organosulfur compound, adsorption from water, and an additional liquid phase adsorption application.

5.2. Mixed Organosulfur Compound Systems

While adsorption of either DBT or DMDBT from the complex matrix of diesel using MCPs has been thoroughly investigated, diesel containing mixtures of organosulfur compounds has yet to be explored. There may be competition for adsorption sites between the different organosulfur compounds present in diesel. The preference of each

MCP for one organosulfur compound over another can be tested using equilibrium and packed bed breakthrough experiments such as those reported in Chapters 2 and 3. Diesel solutions containing relevant amounts of each organosulfur compound should be used in the experiments.

Once the preference for a given MCP for one organosulfur compound over another is determined, optimal systems for the desulfurization of crude fuel can be established. One strategy will be to use mixed bed systems. For example, if MOF-505 is more selective for DBT over DMDBT and UMCM-150 is equally effective at removing DBT and DMDBT, a system consisting of a packed bed of MOF-505 followed by a packed bed of UMCM-150 may be used. In that case, the MOF-505 will first remove the DBT, allowing the UMCM-150 to primarily adsorb the DMDBT.

Another strategy is to use a system containing a guard bed. Activated carbon guard beds have been used effectively with beds of transition metal impregnated zeolites, where the guard bed is responsible for removing the larger organosulfur compounds, allowing the zeolites to effectively remove what remains and increasing the overall capacity of the desulfurization system.[4-7] In the case of MCPs, a zeolite guard bed may be used to first remove the smaller organosulfur compounds, allowing the MCP packed beds to effectively remove the remaining organosulfur compounds.

5.3. Interaction between the Microporous Coordination Polymer and the Organosulfur Compound

Although looking at MCPs that are isostructural (UMCM-150 and its analogs) or supramolecular isomers (UMCM-152 and UMCM-153) can aid in determining the

structural features that increase organosulfur compound adsorption capacity, it would be most beneficial to establish the exact location of the organosulfur compound in the pores of the MCP as this would conclusively aid in determining the most important structural features for achieving large adsorption capacities. An attractive strategy for location of gas phase guest molecules in MCPs is neutron powder diffraction.[8-12] Specifically, preferential binding sites for gases such as H_2 have been determined for various MCPs by loading the MCP with increasing concentrations of D_2. It may be possible to use neutron powder diffraction to locate the guest organosulfur compounds within the pores of the MCPs. Fully deuterated dibenzothiophene (or other organosulfur compound of interest) at varying concentrations can be adsorbed into the MCP, neutron powder diffraction patterns can be obtained and Rietveld refinement of the powder patterns can be used to determine the interaction of the DBT-d_8 with the framework.

It may also be possible to use powder X-ray diffraction to determine the location of the organosulfur compound in the MCP. For example, Rietveld refinement of powder X-ray diffraction patterns has been used to determine the packing of different xylene isomers separated in the liquid phase in the pores of MIL-47 and MIL-53.[13,14]

5.4. Adsorption from Water

Very few cases of the use of MCPs as adsorbents in aqueous systems have been reported,[15-17] even though their zeolite and activated carbon counterparts are often used in aqueous solutions. In Chapter 4, MIL-100 was shown to be a water stable MCP by powder X-ray diffraction and other water stable MCPs have been reported in the literature.[18-21] Because the water stable MCP MIL-100 has such a high capacity for the

adsorption of pharmaceutical compounds from water, it, and other water stable MCPs, may be used for the adsorption and removal of other water contaminants such as pesticides, herbicides, fertilizers, dyes, pharmaceuticals, phenol, aniline, and detergents. In all cases, adsorption capacities can be obtained using the experimental procedures found in Chapter 4.

5.5. Enantiomeric Separations

MCPs have recently been used in liquid chromatographic separations.[22] Mixtures of chemically similar compounds were successfully separated using columns of either MOF-5 or HKUST-1. It may be possible to use this same configuration to successfully separate mixtures of enantiomers using MCPs that have been post-synthetically modified to impart chirality in the MCP. Post-synthetic modification has recently seen a lot of attention in the literature as a means to give functionality to MCPs after synthesis.[23-28] There are two ways that a MCP could be modified to add chiral groups to the MCP: addition of a chiral ligand to the coordinatively unsaturated metal centers of the structure via amine grafting[19,29] or addition of a chiral piece to the organic linker of the structure[27] (Figure 5.2). Chromatographic separation of enantiomers could then be achieved using columns packed with the modified MCPs.

5.6. Conclusions

MCPs have enormous potential for the adsorption of compounds from the liquid phase and can open a gateway to a completely new era in separation/purification sciences. In particular, their superior sorption behavior compared to classical sorbents has

the potential to resolve several long standing problems in the energy-intensive field of separations. A large number of MCPs have been reported and characterized and their use for gas uptake has been extensively evaluated.[30,31] The potential of comparatively few MCPs has been explored for uptake from the liquid phase in spite of the fact that data collected to date prove that these compounds have the potential to be selective sorbents and are kinetically viable for the adsorption of compounds from solution.

The National Science Council Committee on Separation Science and Technology[32] has identified six focus points for further sorption research: 1) Generating improved selectivity among solutes; 2) Concentrating solutes from dilute solutions; 3) Understanding and controlling interfacial phenomenon; 4) Increasing capacity and speed of separation systems; 5) Developing improved process configurations for separation equipment and; 6) Improving energy efficiency in separation. MCPs have the potential to address all of these points and, in some cases, have already exceeded the state of the art of other sorbent classes. It is clear that MCPs act as exquisitely size and shape selective adsorbents and effectively capture molecules from dilute solutions. The ability to change both the metal and the organic linker, with a knowledge of structure derived from crystallography, offers a path towards rationally tailoring interfacial properties. In many cases, MCPs have been shown to outperform benchmark materials such as zeolites and activated carbons by exhibiting higher capacities or more favorable kinetics in certain applications.

Although MCPs have been shown to outperform other microporous materials in liquid phase adsorption applications, it is important to note that issues such as cost have not been taken into account. To date, the cost to make many MCPs prohibits large-scale

production of the material. Further research on inexpensive, easily scalable MCPs that exhibit the stability of zeolites and activated carbons to liquid phase conditions is of the utmost importance. Additionally, separations are highly dependent on the loading of the adsorbents and very few examples have been reported on this issue. Further elucidation of the effect of loading on MCP performance is also necessary before MCPs can make a mark on important industrial applications.

To date, two main areas have been the focus of liquid phase separations by MCPs: separation of enantiomers and the separation of mixtures of chemically different compounds. Within these two areas, two main mechanisms for separation have been prominently observed: size/shape selective separations and chemical separations. In some cases, both mechanisms work together to afford efficient separation of the desired molecules. Going forward with this knowledge, one can imagine the possibility for design of an MCP for a specific separation that would take advantage of either the potential for chemical interactions between the framework and the molecules to be separated or the potential to design a structure with a specific pore size necessary to afford the separation of molecules that themselves are very close in size. With new MCP design, chiral separations with enantiomeric excesses exceeding those that have previously been observed are possible. With further research and effort, MCPs are poised to become leaders in the liquid phase separation of compounds for applications that are very relevant to industry worldwide. Further study is necessary both in the engineering of optimal process configurations and the design of new materials with higher capacities and affinities specifically for industrial applications such that the potential for energy efficiency can be fully realized.

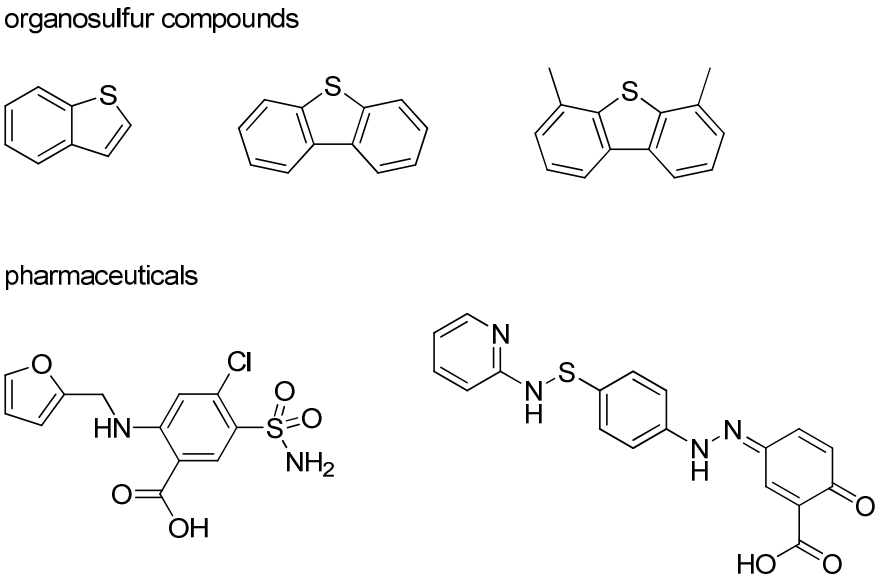

Figure 5.1. Chemical structures of compounds studied for liquid phase adsorption in MCPs in this thesis.

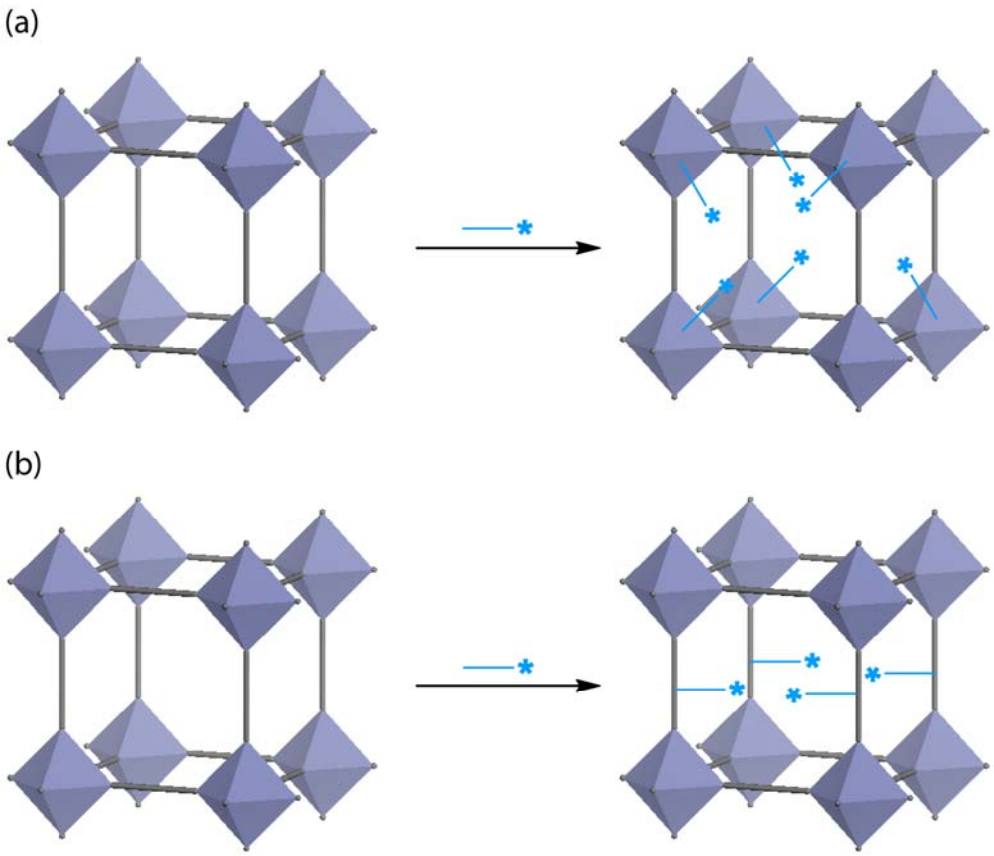

Figure 5.2. Post-synthetic modification of an MCP with a chiral group. (a) Addition of a chiral group to the metal cluster or (b) addition of a chiral group to the organic linker.

5.7. References

(1) Cychosz, K. A.; Wong-Foy, A. G.; Matzger, A. J. *J. Am. Chem. Soc.* **2008**, *130*, 6938-6939.

(2) Cychosz, K. A.; Wong-Foy, A. G.; Matzger, A. J. *J. Am. Chem. Soc.* **2009**, *131*, 14538-14543.

(3) Park, T-H.; Cychosz, K. A.; Wong-Foy, A. G.; Matzger, A. J. *in preparation*.

(4) Hernández-Maldonado, A. J.; Stamatis, S. D.; Yang, R. T.; He, A. Z.; Cannella, W. *Ind. Eng. Chem. Res.* **2004**, *43*, 769-776.

(5) Hernández-Maldonado, A. J.; Yang, R. T. *Ind. Eng. Chem. Res.* **2003**, *42*, 3103-3110.

(6) Hernández-Maldonado, A. J.; Yang, R. T. *Ind. Eng. Chem. Res.* **2004**, *43*, 1081-1089.

(7) Yang, R. T.; Hernández-Maldonado, A. J.; Yang, F. H. *Science* **2003**, *301*, 79-81.

(8) Dincă, M.; Dailly, A.; Liu, Y.; Brown, C. M.; Neumann, D. A.; Long, J. R. *J. Am. Chem. Soc.* **2006**, *128*, 16876-16883.

(9) Dincă, M.; Long, J. R. *Angew. Chem., Int. Ed.* **2008**, *47*, 6766-6779.

(10) Luo, J. H.; Xu, H. W.; Liu, Y.; Zhao, Y. S.; Daemen, L. L.; Brown, C.; Timofeeva, T. V.; Ma, S. Q.; Zhou, H. C. *J. Am. Chem. Soc.* **2008**, *130*, 9626-9627.

(11) Peterson, V. K.; Liu, Y.; Brown, C. M.; Kepert, C. J. *J. Am. Chem. Soc.* **2006**, *128*, 15578-15579.

(12) Xiang, S. C.; Zhou, W.; Gallegos, J. M.; Liu, Y.; Chen, B. L. *J. Am. Chem. Soc.* **2009**, *131*, 12415-12419.

(13) Alaerts, L.; Kirschhock, C. E. A.; Maes, M.; van der Veen, M. A.; Finsy, V.; Depla, A.; Martens, J. A.; Baron, G. V.; Jacobs, P. A.; Denayer, J. E. M.; De Vos, D. E. *Angew. Chem., Int. Ed.* **2007**, *46*, 4293-4297.

(14) Alaerts, L.; Maes, M.; Giebeler, L.; Jacobs, P. A.; Martens, J. A.; Denayer, J. F. M.; Kirschhock, C. E. A.; De Vos, D. E. *J. Am. Chem. Soc.* **2008**, *130*, 14170-14178.

(15) Bai, Y.; He, G. J.; Zhao, Y. G.; Duan, C. Y.; Dang, D. B.; Meng, Q. J. *Chem. Commun.* **2006**, 1530-1532.

(16) Jhung, S. H.; Lee, J. H.; Yoon, J. W.; Serre, C.; Ferey, G.; Chang, J. S. *Adv. Mater.* **2007**, *19*, 121-124.

(17) Wong, K. L.; Law, G. L.; Yang, Y. Y.; Wong, W. T. *Adv. Mater.* **2006**, *18*, 1051-1054.

(18) Choi, H. J.; Dincă, M.; Dailly, A.; Long, J. R. *Energy Environ. Sci.* **2010**, *3*, 117-123.

(19) Demessence, A.; D'Alessandro, D. M.; Foo, M. L.; Long, J. R. *J. Am. Chem. Soc.* **2009**, *131*, 8784-8786.

(20) Férey, G.; Mellot-Draznieks, C.; Serre, C.; Millange, F.; Dutour, J.; Surblé, S.; Margiolaki, I. *Science* **2005**, *309*, 2040-2042.

(21) Férey, G.; Serre, C.; Mellot-Draznieks, C.; Millange, F.; Surblé, S.; Dutour, J.; Margiolaki, I. *Angew. Chem., Int. Ed.* **2004**, *43*, 6296-6301.

(22) Ahmad, R.; Wong-Foy, A. G.; Matzger, A. J. *Langmuir* **2009**, *25*, 11977-11979.

(23) Garibay, S. J.; Wang, Z. Q.; Tanabe, K. K.; Cohen, S. M. *Inorg. Chem.* **2009**, *48*, 7341-7349.

(24) Tanabe, K. K.; Cohen, S. M. *Angew. Chem., Int. Ed.* **2009**, *48*, 7424-7427.

(25) Tanabe, K. K.; Wang, Z. Q.; Cohen, S. M. *J. Am. Chem. Soc.* **2008**, *130*, 8508-8517.

(26) Wang, Z. Q.; Cohen, S. M. *J. Am. Chem. Soc.* **2009**, *131*, 16675-16677.

(27) Wang, Z. Q.; Cohen, S. M. *Chem. Soc. Rev.* **2009**, *38*, 1315-1329.

(28) Wang, Z. Q.; Tanabe, K. K.; Cohen, S. M. *Inorg. Chem.* **2009**, *48*, 296-306.

(29) Hwang, Y. K.; Hong, D. Y.; Chang, J. S.; Jhung, S. H.; Seo, Y. K.; Kim, J.; Vimont, A.; Daturi, M.; Serre, C.; Férey, G. *Angew. Chem., Int. Ed.* **2008**, *47*, 4144-4148.

(30) Kitagawa, S.; Kitaura, R.; Noro, S. *Angew. Chem., Int. Ed.* **2004**, *43*, 2334-2375.

(31) Zhao, D.; Yuan, D. Q.; Zhou, H. C. *Energy Environ. Sci.* **2008**, *1*, 222-235.

(32) National Research Council. *Separation and Purification: Critical Needs and Opportunities*; National Academy Press: Washington, DC, 1987.